Cell Reports
Physical Science

CellPress
OPEN ACCESS

Review

Wood for Application in Electrochemical Energy Storage Devices

Xiaofei Shan,[1] Jing Wu,[1] Xiaotao Zhang,[2] Li Wang,[1] Junli Yang,[3] Zhangjing Chen,[4] Jianfang Yu,[1,*] and Ximing Wang[1,*]

SUMMARY

Nowadays, achieving powerful electrochemical energy conversion and storage devices is a major challenge of our society. Wood is a biodegradable and renewable material that naturally has a hierarchical porous structure, excellent mechanical performance, and versatile physicochemical properties. Wood-based materials and its derivatives are endowed with great potential as resources to fabricate advanced materials for energy storage, flexible electronics, and clean energy. Herein, we comprehensively overview the methodologies applied for the synthesis of various electrochemical energy storage systems and devices (e.g., supercapacitor, battery, catalytic hydrogen evolution, etc.), the strategies for tailoring the structures and conductivity, as well as their impact on electrochemical performance (energy and power density and long-term durability). Finally, an outlook of future opportunities and prospects in the synthesis and application of electrochemical energy storage is also presented.

INTRODUCTION

With the eventual depletion of fossil energy and increasing calling for protection of the ecological system, it is urgent to develop new devices to store renewable energy.[1] Electrochemical energy storage devices (such as supercapacitors, lithium-ion batteries, etc.) have obtained considerable attention owing to their rapid charge-storage capability (i.e., low discharge time: 1–10 s for supercapacitors (SCs), 10–60 min for Li battery (LiB)) and enhanced cyclic stability (SCs > 30 000 h, battery > 500 h).[2,3]

For electrochemical energy storage devices, the electrode material is the key factor to determine their charge storage capacity. Research shows that the traditional powder electrode with active material coating is high in production cost, low in utilization rate of the active material, has short service life and other defects.[4] Therefore, the key to develop electrochemical energy storage devices with low cost and high performance is to find suitable new electrode materials.

For the typical microstructural model with low tortuosity, the vertical microchannels widely exist in natural woods as high pathway for the transportation of water, which has inspired the fabrication of hierarchically structured engineering ceramics with improved mechanical strength and the carbon-based current collectors.[5–7] Wood is the most productive renewable biomass material in nature, which has the advantages of being abundant, sustainable, and biodegradable. Over the years, natural wood has been widely studied for its structure, property,

[1]College of material science and art design, Inner Mongolia Agricultural University, Hohhot 010010, China

[2]College of science, Inner Mongolia Agricultural University, Hohhot 010010, China

[3]CSIRO material science and engineering, Canberra, Australia

[4]Department of Sustainable Biomaterials, Virginia Polytechnic Institute and State University, Blacksburg, VA, USA

*Correspondence: yjf_112@163.com (J.Y.), wangximing@imau.edu.cn (X.W.)

https://doi.org/10.1016/j.xcrp.2021.100654

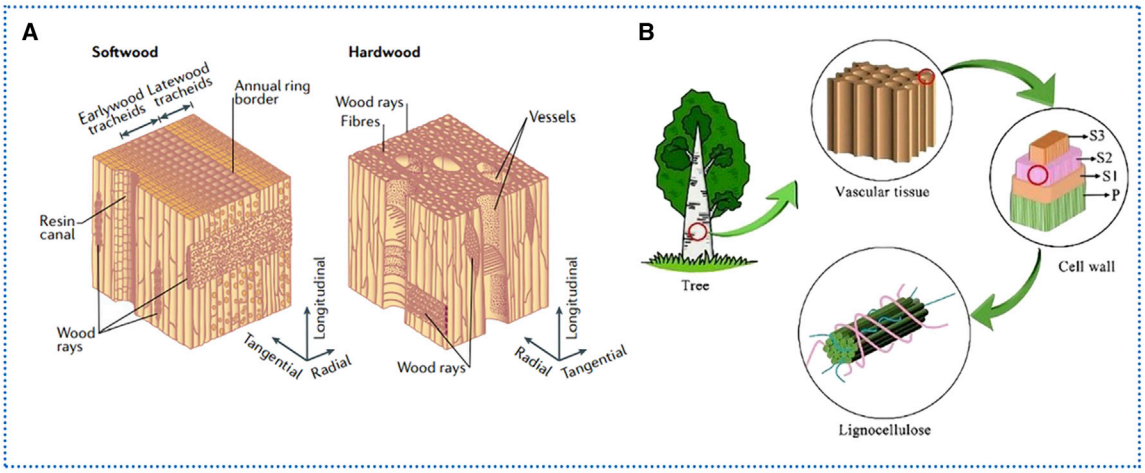

Figure 1. Three dimensional structure of wood

(A) Schematic of wood structure and definition of the three main planes. Reproduced with permission.[8] Copyright 2020, Nature Publishing Group .

(B) Illustration of the hierarchical structure of wood showing different levels.

and function.[8] Wood is a naturally porous material with hierarchical structure, as shown in Figure 1A. It has a fine and complex structure that provides various functions, as a result of billions of years of evolution. It can be used as a kind of precursor of multilayer pore structure. Wood contains a large number of vertically aligned micro channels in tracheids, fibers, and vessels (the diameter ranges 20–140 μm) for transporting water, ions, and nutrients. Wood cell wall components are majorly composed of lignin, hemicellulose, and cellulose. Cellulose molecules are closely packed into crystalline basic filaments with a diameter of 3–5 nm and a length of 30–60 nm, which are widely distributed in the S1, S2, and S3 layers of the secondary wall of the cell wall as mechanical reinforcement phases.[9] These basic filaments wind and deposit layer by layer around the inner cavity of the wood cell, as shown in Figure 1B, giving the cell wall layer a multilayer structure and leading to excellent mechanical properties in wood. Therefore, inspired by this structure, researchers have tried to engineer and utilize wood in making supercapacitors[10–12] and battery electrodes,[13–16] and as a resource in water treatment.[17–19]

For energy storage devices, especially high-mass-loading electrodes, active materials could be delaminated from current collectors, and the high tortuosity of electrodes may hinder the ion transport and extend ion diffusion pathway, leading to limited active material utilization. Moreover, the binder may block the electrons transfer and bring in some "dead" sites which cannot support electrochemical reactions.[20] The hierarchically porous and low-tortuosity structure of wood have abundant open channels, which facilitates solution permeation, ion diffusion, and desorption of gas bubbles.[13,19] This hierarchical porous structure is a suitable feature for making electrode materials. In recent years, researchers at home and abroad have taken advantage of this feature (three-dimensional porous structure, a large number of vertically arranged straight channels and low bending) and applied wood in the field of electrochemical energy storage. In this paper, we reviewed the latest research progress in the application of wood material for electrochemical energy storage, primarily in supercapacitors and various types of batteries, and finally discuss the existing problems and future prospects of developing wood-based energy storage materials.

DIFFERENT TYPES OF WOOD STRUCTURES

With the development and utilization of novel materials, people have carried out a series of physical / chemical treatments on wood and obtained many different structural types of wood-derived materials, such as densified wood,[21] transparent wood[22,23] and sponge wood.[24] In the future, they will play their respective roles in different application fields.

Structure and properties of wood-derived materials

Natural wood is a low-cost and abundant material and has been used for millennia as a structural material for building and furniture construction. However, the mechanical performance of natural wood (its strength and toughness) is unsatisfactory for many advanced engineering structures and applications. In order to improve this phenomenon, Song et al. partially removed lignin and hemicellulose from the natural wood via a boiling process in an aqueous mixture of NaOH and Na_2SO_3, followed by hot-pressing,[21] leading to the total collapse of cell walls and the complete densification of natural wood, highly aligned cellulose nanofibers (Figure 2A). This high-performance structural material has a specific strength higher than that of most structural metals and alloys—more than tenfold increase in strength, toughness, and ballistic resistance—and has greater dimensional stability (Figure 2B), making it a low-cost, high-performance, lightweight alternative.

Transparent wood has emerged due to its unique hierarchical structure,[25,26] high specific strength,[27,28] and favorable light=management properties.[29,30] It is considered a promising structural and light-management material for energy-efficient engineering applications. Zhu et al. removed lignin from wood—the yellowish wood block becomes white due to the light scattering and the lack of light absorption by lignin. The lumina in the delignified wood now can allow fast infiltration of a refraction index-matching polymer to decrease the light scattering, thus leading to a highly transparent wood composite (Figures 2C and 2D).[22] However, the solution-based delignification process that is used to fabricate transparent wood generally consumes large amounts of chemicals and energy. Therefore, Xia et al. modified the wood's lignin structure by using a solar-assisted chemical brushing to produce optically transparent wood.[23] This method preserves most of the lignin to act as a binder, providing a robust wood scaffold for polymer infiltration, while greatly reducing chemical and energy consumption as well as processing time.

An efficient collection and recovery of high-viscous crude oil from oil spillage in an environmentally friendly way is extremely important for water remediation. Therefore, Chao et al. fabricated a high-compression wood sponge by selective removal of lignin and hemicellulose via a two-step chemical treatment process,[24] further decorated *in situ* with reduced graphene oxide for photothermal conversion thermogenesis to lower the viscosity of crude oil for better fluidity and treatability(Figures 2E–2G). Compressible properties of sponge wood enabled simple recovery of adsorbed crude oil by mechanical compression, so as to achieve efficient adsorption of high-viscosity crude oil illumination and recovery.

Structure and characteristics of wood in energy storage devices

In recent years, inspired by the vertical microchannels in natural wood as the highway for water transport, some novel wood-based materials for energy storage devices have been developed.[31] There are two most common treatment methods for wood with such uses—wood high-temperature carbonization treatment and wood flexibility treatment.[32]

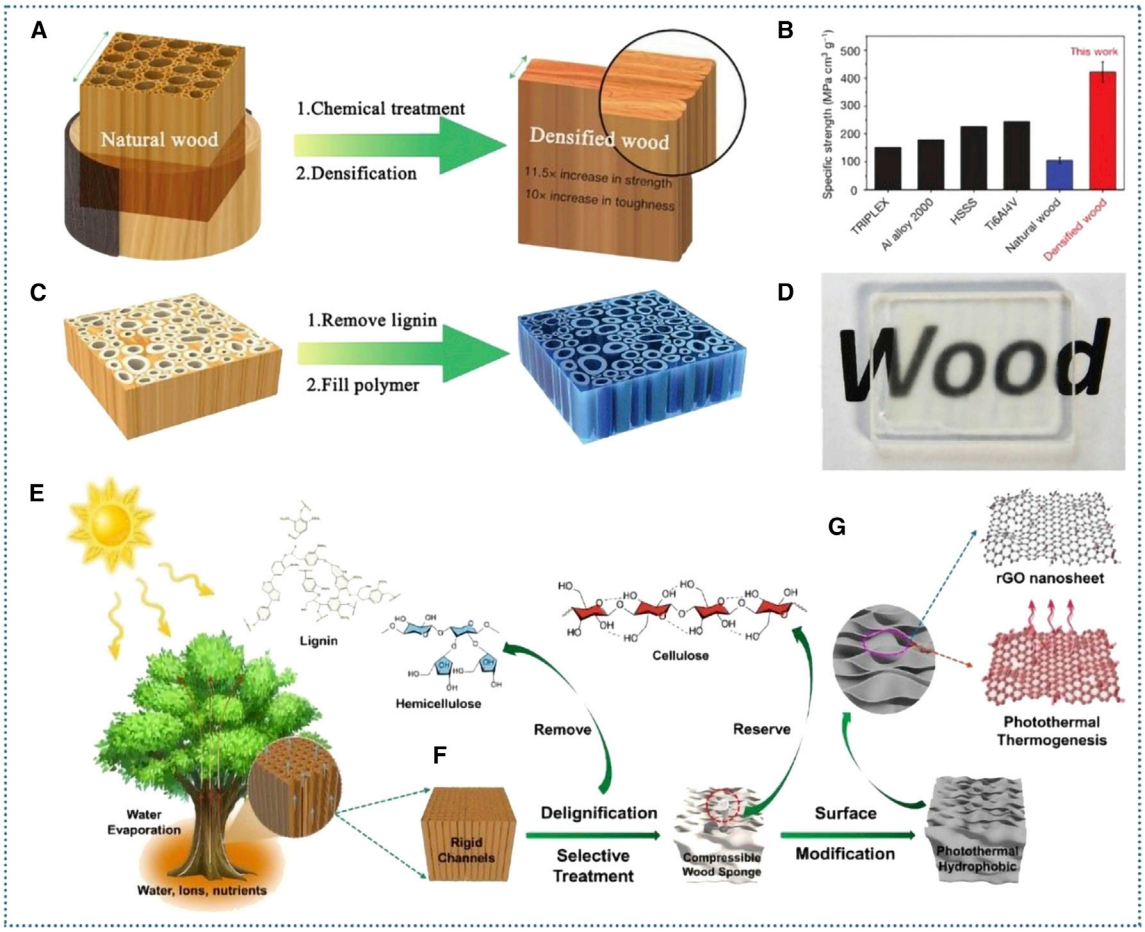

Figure 2. Structure and properties of different types of wood

(A) Schematic of the top-down, two-step approach to transforming bulk natural wood directly into superstrong, densified wood.

(B) Specific tensile strength of the resulting densified wood. Reproduced with permission.[21] Copyright 2018, Nature Publishing Group.

(C) Schematic to show the fabrication of transparent wood.

(D) A photograph of the transparent wood. Reproduced with permission.[22] Copyright 2016, Wiley-VCH.

(E) Graphical illustration of naturally grown tree and the solar-motivated evaporation process.

(F) Schematic illustration of the fabrication of OTS-rGO-WS from NW through WS.

(G) Illustration of photothermal effects of *in situ* reduced graphene oxide coating over OTS-rGO-WS. Reproduced with permission.[24] Copyright 2020, Elsevier BV.

Wood-derived carbon can be obtained by high-temperature carbonization. As shown in Figure 3A, carbonized wood (CW) still retains the three-dimensional porous structural characteristics of natural wood,[33] and the material obtained by this treatment method has high conductivity, which successfully solves the problem of wood insulation, thus greatly broadening the application range of wood. Making full use of the natural advantages of high porosity, three-dimensional structural-material–fiber support, combined with other treatment methods, has become a new direction in the field of conductive energy storage.

Through a chemical treatment method, natural wood can be changed to flexible wood. As shown in Figures 3B and 3C, such superflexibility is attributed to both physical and chemical changes of the natural wood, particularly in the formation of the wavy structure formed by simple delignification induced by partial removal of lignin/hemicellulose. The flexible wood, which inherits its unique 3D porous

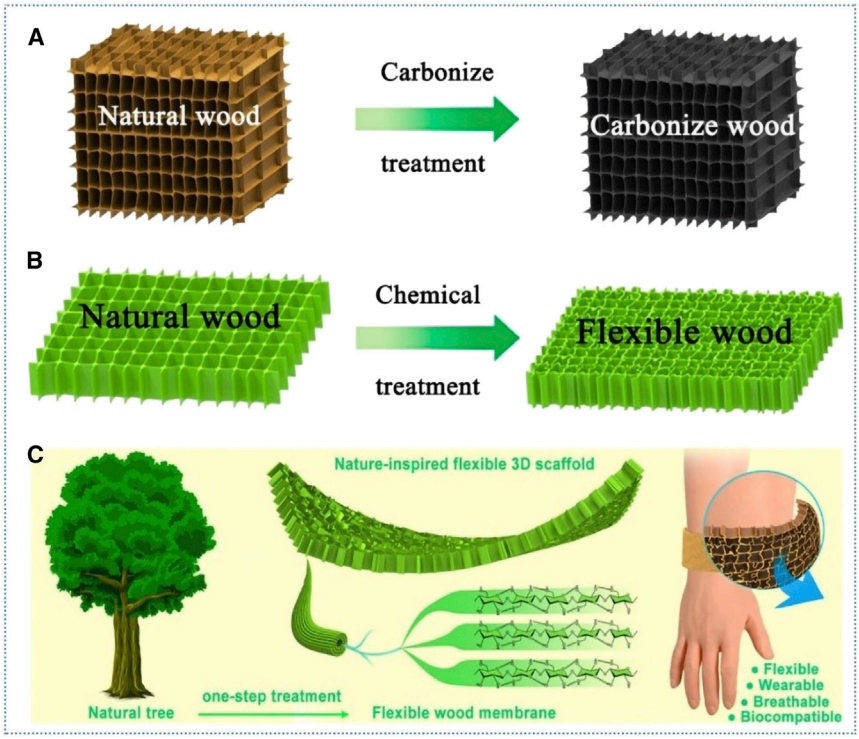

Figure 3. Pretreatment and application of wood

(A) Structural evolution of wood after carbonization. Reproduced with permission.[33] Copyright 2018, Elsevier.

(B) Structural evolution of wood after chemical treatment.

(C) Schematic diagram of flexible wood for wearable devices. Reproduced with permission.[32] Copyright 2017, American Chemical Society.

structure with aligned cellulose nanofibers, biodegradability, and biocompatibility from natural wood, combined with the superflexibility imparted by a simple chemical treatment,[32] can be applied to flexible electrodes and sensors.

APPLICATION OF WOOD IN SCs

SCs are mainly composed of electrode, diaphragm, electrolyte, current collector, and shell. They have the characteristics of being safe and environmentally friendly, and of rapid charge-discharge, high energy density and power density, ultralong life cycle, and wide-working temperature range.[34] The electrode materials play a decisive role in the entire electrochemical performance of the SCs.[35] The three-dimensional (3D) straight channel structure of wood can greatly enhance the transmission of ions and electrons, making wood a candidate as a natural electrode material. In recent years, many researchers have applied wood to produce supercapacitor energy storage devices. Key parameters in these studies are summarized in Table 1 for comparison.

CW as electrode

The capacitance of an electric double layer capacitor (EDLC) is highly dependent on the specific surface area (SSA) of the carbonaceous materials, especially ultra-microporous surface area (ultra-SSA).[36] Unfortunately, commercial carbon material with high porosity and broad pore distribution will lead to low normalized and volumetric capacitance.[37] CW is a kind of carbon derived from wood and it is obtained by

Table 1. Summary of key parameters of various wood-based materials for SCs

Ref.	Wood species	Electrode	Carbonization condition	Activation condition	Surface area [m^2g^{-1}]	Active mass loading	Electrochemical performance	Electrolyte	Cycles (%)
39	Beech wood	CW	N_2 (800°C, 2h)	–	44	–	39.2 Wh kg^{-1} at 200 mA g^{-1}	KOH (2M)	2,000 (~97%)
	Pine wood				76		45.6 Wh kg^{-1} at 200 mA g^{-1}		
	Sandal wood				38		32.9 Wh kg^{-1} at 4000 mA g^{-1}		
40	Poplar wood	m-WCM	N_2 (900°C, 6h)	HNO_3	416	–	234F g^{-1} at 5 mA cm^{-2}	KOH (2M)	2,000 (~97%)
41	Poplar wood	AWC	N_2 (500°C,1h+ 1,000°C,2h)	Air (450°C,1h)	663 ± 10	–	235 F g^{-1} (6.85 F cm^{-2}) at 1 mA cm^{-2};	KOH/PVA gel	10,000 (~96%)
48	Bass wood	TARC	N_2 (950°C, 2h)	NH_3	1438	–	704 F g^{-1} at 0.2 A g^{-1};135 F g^{-1} at 0.2 A g^{-1};15.2 Wh Kg^{-1} at 0.2 A g^{-1}; 8.9 Wh Kg^{-1} at 3234 W Kg^{-1}	KOH (4M)	5,000 (~94%)
54	Fir wood	Wood/ RGO	–	–	–	0.68 mg cm^{-2}	151 F g^{-1} at 1 m V s^{-1};areal power density: 0.47 mW cm^{-2}	PVA/H_3PO_4 gel	5,000 (~98.9%)
55	Birch wood	wood/ AC	Ar (400°C, 2.5h)	NaOH	3300	–	AC synthesized at 600°C is 330 F g^{-1}	H_2SO_4	no notable loss after 10. 000 cycles
61	Balsa Wood	LFW/ PANI	–	–	–	30wt%	800 F g^{-1};41 Wh kg^{-1}	H_2SO_4 (1M)	5,000 (~96%)
65	Fir wood	Lig/PPy-wood	–	–	–	8 mg cm^{-2}	1062 mF cm^{-2} at 1 mA cm^{-2}; 47.2 lWh cm^{-2} at 400 lWc m^{-2}	H_2SO_4 (1M)	5,000 (~82.1%)
75	Bass wood	MnO_2/ WC	Ar (1,000C, 6h)	CO_2	–	75 mg cm^{-2}	3600 mF cm^{-2} at 1 mA cm^{-2}; 1.6 mWh cm^{-2}	Na_2SO_4(1M)	10,000 (~93%)
78	Poplar wood	$Co(OH)_2$/CW	N_2 (1,000°C, 2h)	–	568.13	5.7 mg cm^{-2}	3.723 F cm^{-2} at 1.0 mA cm^{-2}; 1.568 F cm^{-2} at 30 mA cm^{-2}; 0.69 mWh cm^{-2}(10.87 Wh kg^{-1}) at 1.126 W cm^{-2}(17.75 W kg^{-1})	KOH (2M)	10,000 (~85%)
82	Balsa wood	PWC/ MnO_2/ GQDs	N_2 (1,000, 2h)	–	–	15mg	2712 mF cm^{-2} at 1.0 mA cm^{-2}; 1075 mF cm^{-2} at a current density of 20 mA cm^{-2}	Na_2SO_4(1M)	2,000 (~95.3%)
86	Light wood	CLFW/ Co-CoS	(800°C, 6 h)	–	–	–	610 μWh cm^{-2};192 mW cm^{-2}	Li_2SO_4 (1.5 M)	–
93	Light wood	CLFW/ Ni-NiS/V	(800°C, 6 h)	–	–	–	38 Wh kg^{-1} (56 kW kg^{-1}), 687 μWh cm^{-2} (202 mW cm^{-2}), 58 Wh L^{-1} (39 kW L^{-1}) at 1 mA cm^{-2}	Li_2SO_4	–

high-temperature heat treatment of wood under the condition of being oxygen free. It has high SSA and abundant porosity, and the hierarchical porous structure provides a fast channel for the transmission of electrons and ions. It can be directly used as a self-supporting electrode without additional conductive agent and adhesives. Therefore, CW is an ideal choice for high-performance SC electrodes.[38] However, the electrochemical performance of the CW, when directly used as a SC electrode, is not ideal. Therefore, it is necessary to activate the CW to further improve the specific capacitance of SCs.

Teng et al. prepared a 3D network electrode with interconnected micro-channels by carbonizing wood in N_2 atmosphere.[39] From charge-discharge cycling in a KOH electrolyte solution, an energy density of 45.6 Wh kg^{-1} (discharge current of 200 mA g^{-1}) and a power density of 2000 W kg^{-1} (discharge current of 4,000 mA g^{-1}) were obtained, and the specific capacitance retention rate is 99.7% after 2,000 cycles. These remarkable results demonstrate an exciting potential for the CW materials as inexpensive, high-performance SC electrodes. Liu et al. prepared a surface modified porous wood carbon monolith (m-WCM) electrode with excellent SC performance by carbonization of wood and surface modification with HNO_3 solution.[40] The electrode has an hierarchical porous structure and large porosity. The obtained m-WCM was studied as electrodes for supercapacitors and exhibited excellent electrochemical performance compared with typical activated carbon (AC) and ordered mesoporous carbon (CMK-3). Gravimetric capacitance for m-WCM is 234 F g^{-1}, with 97% specific capacitance retained after 2000 cycle tests; this is mainly due to surface functional groups that were introduced onto the surface of the m-WCM after surface modification. These chemical groups not only improve the hydrophilicity of m-WCM, but also provide pseudocapacitance to some extent as the following redox reactions. Zhang et al. report a facile, low-cost, and efficient methodology by two-step thermal treatment for natural wood bulks to prepare activated wood carbon (AWC) used as freestanding ultrathick electrodes of symmetric SCs (Figure 4A).[41] Thanks to the straight channels with low tortuosity, the oxygen-containing functional groups, and the fabrication of a thick electrode, the optimal electrode (AWC) exhibits outstanding SC performances of 235 F g^{-1} (6.85 F cm^{-2}) at 1 mA cm^{-2} (Figure 4B), more than twice than the CW electrode (107 F g^{-1}). The energy density for the AWC electrode can achieve 32.6Wh kg^{-1} (0.95 mWh cm^{-2}), at power density of 17.1 kW kg^{-1} (0.5 W cm^{-2}) (Figure 4C). Furthermore, the AWC ultrathick electrode also exhibits an excellent cycling stability, retaining a capacitance of 96% of initial value even at a high current density of 30mA cm^{-2} after 10000 cycles (Figure 4D). Therefore, from previous studies, we can conclude that CW is a kind of natural biomass material suitable for the SC electrode, and its application as an electrode material is very likely to be promoted in future. Furthermore, the CW can be activated to some extent, which can not only make micro pores on the CW to increase the SSA, but also introduce other active groups to increase the reaction active sites, so as to improve the energy storage efficiency of SCs.

Wood-based heteroatom-doped electrode

Heteroatom-doped carbon materials, as metal-free catalysts, have emerged as efficient alternatives for boosting oxygen reduction reaction (ORR), owing to their competitive electrochemical activity, high conductivity, cost effectiveness, and satisfactory durability.[42,43] Meanwhile, dimensional design of carbon materials with hierarchically porous structure could favor prompt mass transport and yield up abundant accessible active sites.[44–47] Therefore, Tang et al. prepared an N, S co-doped carbon skeleton (TARC-N) for the SC electrode by impregnating the delignified basswood with trithiocyanuric acid (TA) and carbonizing it.[48] the preparation process is

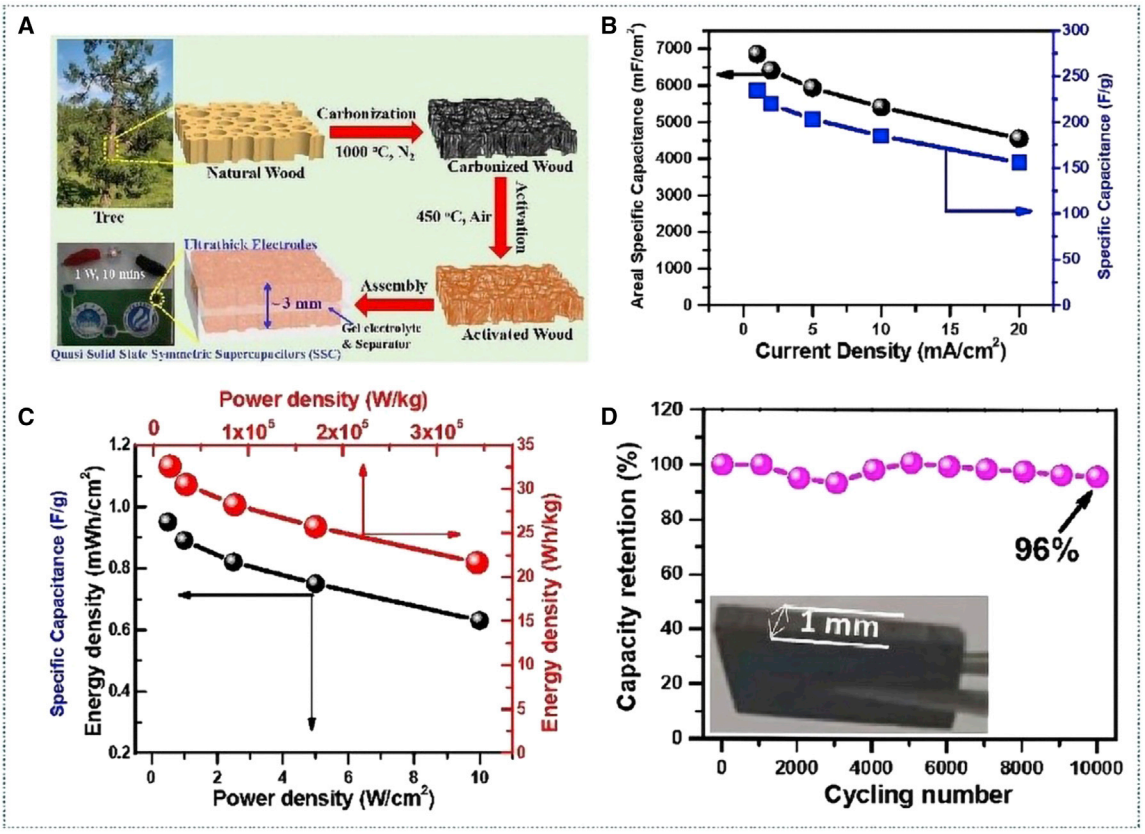

Figure 4. Preparation process and properties of AWC electrode

(A) Construction of a quasi-solid-state symmetric supercapacitor (SSC) based on activated wood carbon (AWC) monoliths as freestanding ultrathick electrodes.

(B) The areal and gravimetric capacitances based on different discharge current densities.

(C) Power / energy densities of the supercapacitor.

(D) Cycling stability of the AWC electrode at 30 mA cm^{-2} (inset is a typical photograph of thick electrode). Reproduced with permission.[41] Copyright 2020, Royal Society of Chemistry.

shown in Figure 5A. It provides an impressive gravimetric specific capacitance (Cs) of 704 F g^{-1} at 0.2 A g^{-1} (Figure 5H). The capacitance retained 94% of the initial capacitance after 5000 charge-discharge cycles at a current density of 2 A g^{-1}(Figure 5C). This is mainly because the multispace straight-channel structure of wood ensures fast electrochemical kinetics, which is conducive to the transport of electrolyte ions. More importantly, heteroatoms doping enhances the hydrophilicity and polarity of wood carbons, thus introducing functional groups to achieve pseudocapacitive behavior. The Zn-air battery using TARC-N as an air-cathode catalyst demonstrated an open-circuit voltage of 1.47 V, a current density of 330 mA cm^{-2} at 0.7 V, a peak power density of 241 mW cm^{-2} and a high energy density of 945.2 Wh kg_{Zn}^{-1} at 10 mA cm^{-2}, in conjunction with an outstanding stability (over 100 h after 4 mechanical charges).

Wood-based composite electrode

At present, electrode materials are mainly divided into carbon materials,[51] conductive polymers,[52] metal oxides,[53,54] etc., according to their properties. Among them, carbon materials not only have the advantages of being abundant and involving cheap production costs, easy operation, no toxicity, good electronic conductivity, high chemical stability, wide-working temperature range and so on, but they also

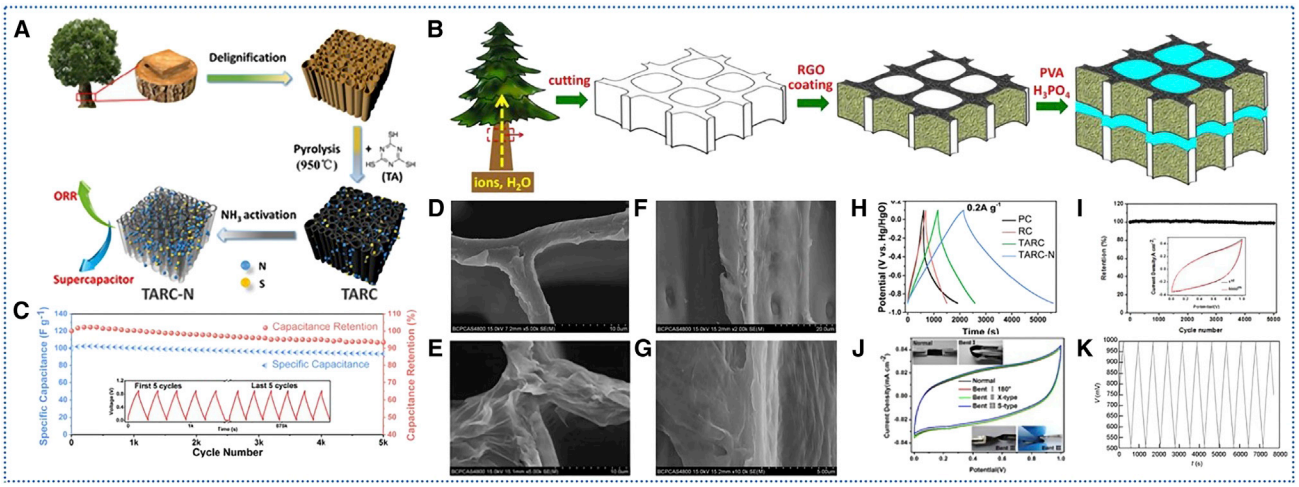

Figure 5. Preparation technology and properties of materials

(A) Graphical illustration for the fabrication process of N, S co-doped wood carbons. Reproduced with permission.[48] Copyright 2018, Elsevier.

(B) Schematic diagram of the preparation processes of native WTSS, WTSS-RGO, and its supercapacitor. Reproduced with permission.[49] Copyright 2015, Korean Institute of Metals and Materials.

(C) Cycling stability for 5,000 cycles at a current density of 2 A g^{-1}, the inset shows the charge-discharge profiles obtained from first and last 5 cycles. Reproduced with permission.[48] Copyright 2018, Elsevier.

(D) SEM image of WTSS.

(E) SEM image of the WTSS-RGO electrode at the same magnification of frame (D).

(F) Cross-sectional SEM images of the WTSS-RGO electrode.

(G) Shows the wrinkled textures of the inner wall surface of the tracheid cell wall. Reproduced with permission.[49] Copyright 2015, Korean Institute of Metals and Materials.

(H) Galvanostatic charge-discharge (GCD test at 0.2 A g^{-1}) from the first cycle for PC, RC, TARC and TARC-N. Reproduced with permission.[48] Copyright 2018, Elsevier.

(I) Cyclic stability of the WTSS-RGO supercapacitor.

(J) Comparison of the CV curves under normal and bent states. Reproduced with permission.[49] Copyright 2015, Korean Institute of Metals and Materials.

(K) Cyclic stability of SC with the electrodes made from the AC. Reproduced with permission.[50] Copyright 2017, Zhongguo Kexueyuan.

have higher SSA and a highly porous structure.[55] The above characteristics support the construction of an electric double-layer capacitor structure and play an important role in electrochemical energy storage. Conductive polymer is a kind of fast reversible redox reaction of active material during charge-discharge, and an n-type or p-type doping is produced on polymer film quickly, so as to store high-density charge. Metal oxides produce capacitors through highly chemical adsorption and desorption or redox reactions through active substances. Conducting polymers and metal oxides are often used in the faradaic pseudocapacitor. The 3D porous structure of wood not only plays a role in the storage of electrolyte, but also provides sufficient space for the loading of active electrode materials. Therefore, the electrochemical performance of supercapacitors will be greatly improved by growing active materials on wood for SC electrodes.

Based on the structural characteristics of wood and many advantages of carbon materials, researchers are inspired to combine the two to prepare SC electrodes with high-energy storage, direct channel, and low cost. Lv et al. used wood transverse section slice (WTSS) as flexible scaffold and reduced graphene oxide (RGO) with excellent conductivity and rich SSA as active material to create a flexible electrode,[49] and assemble the SC, as shown in the Figure 5B. The areal capacitance of the electrode reaches 102 mF cm^{-2} at low scanning rate of 1 mV s^{-1}; at the sweep rate of 50 mV s^{-1}, the capacitance barely decreased after 5,000 cycles, and the retention retained the high value of 98.9% (Figure 5I). The capacitance performance of

different mechanical deformation is studied. The three bent states (180°, X-type, and S-type) had almost no effect on the capacitive behavior of the flexible device (Figure 5J). This is mainly due to the fact that RGO nanoparticles adhere to the cell wall and strongly attached to the WTSS, which are distributed throughout its macroporous framework to form a conductive honeycomb network (Figures 5D–5G). On the other hand, the above properties are mainly due to the porous 3D honeycomb structure of WTSS, which provides an additional and continuous transport path for the active RGO and electrolyte phase, so that the electrode shows excellent performance. In addition, Volperts et al. used wood precursor as raw material and NaOH as activator, the wood-based AC with high efficiency adsorption performance was synthesized and used as the electrode of SCs in sulfuric acid electrolyte.[50] The test shows that the SC made using the AC synthesized at 600°C has a capacitance of 330 F g^{-1}, and the SC device has no notable loss of its performance after 10,000 cycles (Figure 5K). In addition to the above situation, the combination of wood and a variety of carbon materials can achieve ideal results. For example, Lv et al. prepared a new type of ultra-thin, flexible light wood/nano carbon composite electrode by combining wood slices with two kinds of nano carbon materials graphene (RGO) and carbon nanotubes (CNT) as flexible support materials and carrier materials.[56] The results show that there is no obvious interface between both RGO and CMWCNT nano-carbon materials and veneers, indicating that there is a strong adhesion between them, which is due to the hydrogen bonding between them. The current of the electrode keeps stable under different bending degrees, and the bending stress has little effect on its conductivity. Therefore, the wood should be treated properly and used as the support material of flexible electrode. It is expected that flexible composite electrode made by mounting nano carbon materials onto a wood composite 3D structure frame would find applications in products such as flexible energy storage devices and flexible wearable devices.

In recent years, polyaniline (PANI), polypyrrole (PPy), polythiophene (PTH) and other conductive polymers are often used as active electrode materials for energy storage. It has reversible redox reaction and can provide good faradaic pseudocapacitance. However, when the capacitor is in the working state, the volume of conductive polymer changes sharply and the conductivity decreases, which results in the electrode materials having the disadvantages of poor cycle stability and rapid capacitance loss. Researchers subsequently studied to combine conductive polymers with carbon nanostructured materials. In order to improve the electrochemical performance, the structure of carbon material is used to limit the volume change of conductive polymer during the charge-discharge cycle.[57] Researchers also studied to make SC electrodes by combining wood with a conductive polymer.[58–60] The combined effects of these two materials have produced encouraging results.

PANI, as a conducting polymer pseudocapacitor material, has high pseudocapacitance. It has been widely studied and used because of its availability, simple synthesis process, and chemical and environmental stability. Xiong et al. used lignin-free wood (LFW) as a substrate to load aniline monomer, and then LFW @ PANI was prepared by self-polymerization of aniline monomer in LFW, and the composite was used as an electrode of SCs.[61] The manufacturing process is shown in Figure 6A. The electrode shows excellent capacitance characteristics, the specific capacitance of the electrode is 800 F g^{-1} and 192 F cm^{-3}(Figures 6G and 6H). After 5,000 cycles, the cycle stability of the electrode is as high as 96% (Figure 6I); the energy efficiency is more than 80% (Figure 6J). The energy density is 41 Wh kg^{-1}, and the power density is 68 kW kg^{-1}. This is mainly because the natural porous structure of wood and the 3D porous structure of PANI nanofibers provide faster channels for the transport

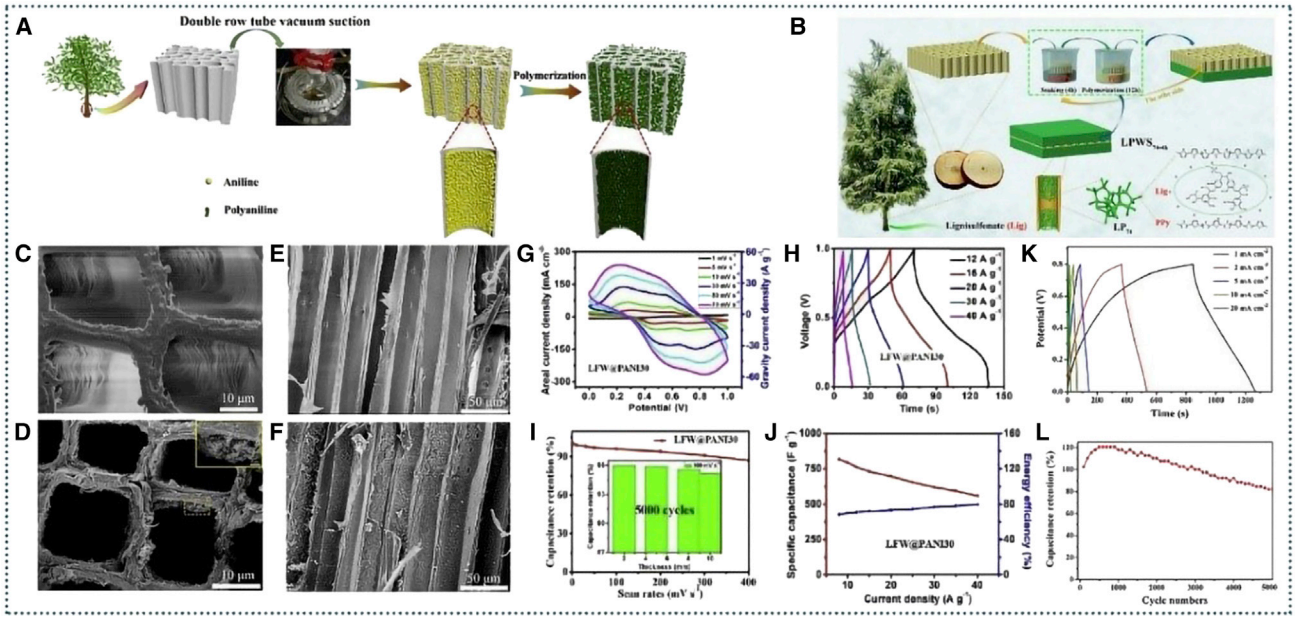

Figure 6. Preparation technology and properties of materials

(A) Shows the fabrication procedure of the LFW@PANI hybrid. Reproduced with permission.[58] Copyright 2020, Elsevier.

(B) Schematic illustration of preparation process of the all-in-one and mechanically stiff $LPWS_{74\text{-}4h}$.

(C) SEM images of natural wood cross section piece.

(D) The image cross section of the $LPWS_{74\text{-}4h}$.

(E) SEM images of natural wood longitudinal section piece.

(F) The image longitudinal section of the $LPWS_{74\text{-}4h}$. Reproduced with permission.[62] Copyright 2021, Springer Netherlands.

(G and H) The comparison of the (G) CV curves and (H) GCD curves of the LFW@PANI 30 hybrid under different scan rates and current densities, respectively.

(I) The capacitance retention of the LFW@PANI 30 hybrid under various scan rates.

(J) The gravimetric specific capacitance and energy efficiency of the LFW@PANI30 as a function of the current densities. Reproduced with permission.[58] Copyright 2020, Elsevier.

(K) The galvanostatic charge-discharge (GCD) curves at the different current density (1–20 mA cm^{-2}).

(L) The cycling stability at a current density of 10 mA cm^{-2}. Reproduced with permission.[62] Copyright 2021, Springer Netherlands.

of electrolyte ions, thus showing good electrochemical behavior. PPy is widely used as electrode materials in supercapacitors because of the promising characteristics of offering easy synthesis, being environmentally friendly, and providing good conductivity and high capacitance.[62–64] Here, a novel integrated and mechanically stiff all-in-wood SC is constructed with lignosulfonate/polypyrrole (Lig/PPy) hydrogel embedded in wood by *in situ* polymerization of pyrrole in both sides of the wood piece in the Lig/Py solution, as shown in Figure 6B.[65] Lignosulfonate (Lig), as the main derivative of lignin, is a component of wood.[66] The formed Lig/PPy hydrogel can be tightly attached in the wood because of the strong interaction between Lig and wood. Moreover, Lig is electroactive as its massive phenol groups can induce reversible redox reaction.[66,67] After polymerization, the surface and the well of the vertical channel of $LPWS_{74\text{-}4h}$ are rough, and the diameter of the vertical channel increased significantly, indicating the successful attachment of Lig/PPy hydrogel (LP_{74}) in wood (Figure 6C–6F). The $LPWS_{74\text{-}4h}$ exhibits a high areal capacitance of 1,062 mF cm^{-2} at the current density of 1 mA cm^{-2}, which is much higher than other previously reported all-in-one super-capacitors (Figure 6K). The $LPWS_{74\text{-}4h}$ can maintain 82.1% of the initial capacitance after 5,000 cycles (Figure 6L). The $LPWS_{74\text{-}4h}$ exhibits a high areal energy density of 47.2 μWh cm^{-2} at the areal power density of 400 μW cm^{-2}. Meanwhile, the $LPWS_{74\text{-}4h}$ also shows impressive mechanical stiffness with a maximum compressive strength of 71 MPa. This is mainly due to the unique

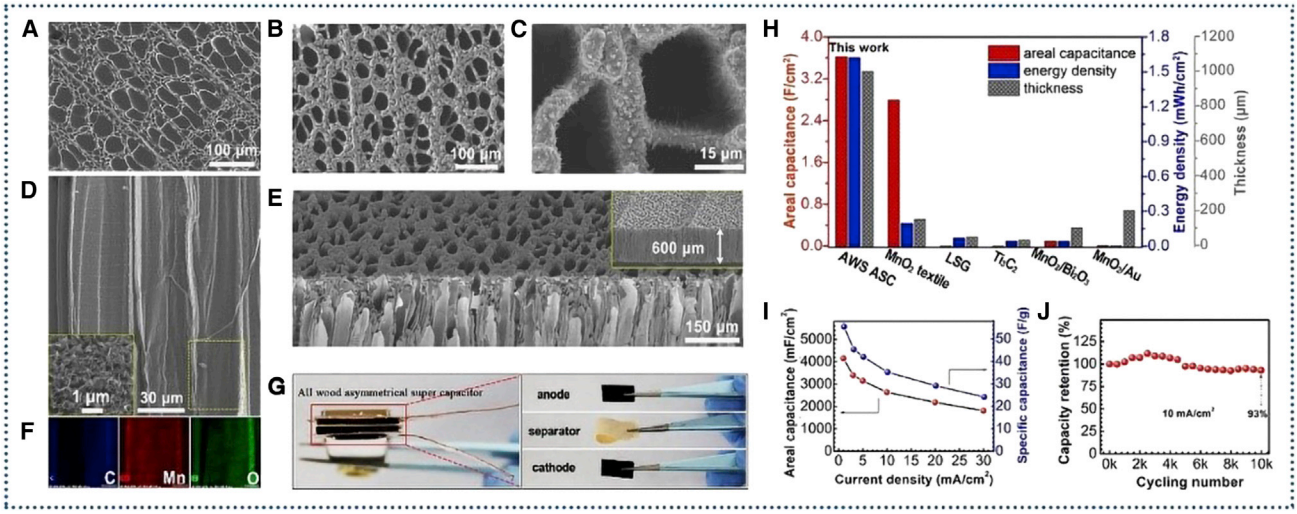

Figure 7. Microstructure and properties of materials

(A) SEM image for the raw wood carbon.

(B–E) SEM images for the wood carbon/MnO_2 (MnO_2@WC) composite: (B) top view, (C) magnified image of (A), (D) channels, inset in (D) shows the nanosheets *in situ* grown inside the channel, and (E) top and cross-section view, inset in e shows the thickness of the MnO_2@WC composite.

(F) Element mapping images of C, Mn and O inside the channel.

(G) Pictures of the AWC anode, wood separator and MnO_2@WC cathode, and picture of the all-wood structured all-solid state asymmetric supercapacitor.

(H) Areal capacitance, energy density and electrode thickness of the all-wood-structured ASC (AWS ASC) compared with the previous reported electrode materials.

(I) Rate performances of MnO_2@WC.

(J) Cycling performance of ASC. Reproduced with permission.[75] Copyright 2017, Royal Society of Chemistry.

hierarchical porous structure of wood, which not only can ensure high mass loading of the electro-active material, but also can relieve the swelling and shrinking of the Lig/PPy chains;[68] on the other hand, the Lig/PPy hydrogel embedded with the conductive porous network structure can provide high pseudocapacitance. Because the capacitor has good electrochemical performance and excellent mechanical properties, it has the potential to be applied in the next generation of green and structural energy devices, and further expanded in the field of super capacitor energy storage.

Compared with carbon materials, transition metal oxides (such as manganese dioxide (MnO_2), cobalt hydroxide ($Co(OH)_2$)) and a few other materials have attracted a lot of interest at home and abroad because of their high theoretical capacity and low cost. Among them, MnO_2 has not only abundant sources, low cost, and polycrystalline structure, but its theoretical specific capacitance is also as high as 1,370 F g^{-1};[69] therefore it has been widely used in energy storage devices. However, as a semiconductor material, MnO_2 has low conductivity and high internal resistance, which leads to its actual specific capacitance being only about 200–450 F g^{-1},[70] and its capacity decreases rapidly with the increase of the charge-discharge rate, and its rate performance is very poor. In order to improve the actual specific capacitance, electrical conductivity, and rate performance of MnO_2, many researchers have combined MnO_2 with high conductivity materials at nano scale.[71–74] For example, Chen et al. have grown MnO_2 *in situ* on the wood carbon block to produce the MnO_2@WC electrode materials by the typical anodizing method.[75] After loading MnO_2, almost all of the small channels in the CW cross section were filled (Figures 7A and 7B). A large number of needle-like nanosheets were grown on the surface of the wood carbon and inside its channels (Figure 7C). Figures 7D and 7E show that the MnO_2

nanosheets were uniformly grown inside the channels over the entire MnO_2@WC slice. The uniform distribution of MnO_2 nanosheets can be further confirmed by the C, O, and Mn element mapping images (Figure 7F). A remarkably high areal capacitance of 4,155 mF cm^{-2} can be achieved at 1 mA cm^{-2}(Figure 7I), indicating an excellent rate of performance of the MnO_2@WC electrode. A novel all-wood structure which was low bending, safe, and biodegradable) was designed for asymmetric SCs (ASC) with activated wood carbon (AWC) as the anode, thin wood membrane as the separator, and MnO_2/wood carbon (MnO_2 @ WC) as the cathode (Figure 7G). The thickness of the SCs is up to 1 mm. The direct low-tortuosity channels and high electronic and ionic conductivity enable the ASC device to exhibit a high areal capacitance (3.6 F cm^{-2}), high energy/power densities (1.6mWh cm^{-2} at 1044mW cm^{-2}) (Figure 7H). After a long-term charging/discharging cycling at 10 mA cm^{-2} for 10 000 cycles, 93% of the capacitance can still be retained (Figure 7J). Apparently, by only altering the electrode design and device structure without changing chemical compositions of the electrode materials, one can achieve straight channels, low tortuosity and high ionic and electronic conductivities, and high structural stability without the concern of electrode deformation. This certainly provides a promising and broader future for the development of high-performance energy storage devices, not limited to superelectric containers.

Besides, cobalt hydroxide [$Co(OH)_2$] is one of the most promising candidates due to its large specific capacitance of 3,460 F g^{-1}, low cost, and abundant availability.[76] However, the obtainable capacitances of $Co(OH)_2$-based capacitors are typically lower than their theoretical value.[77] Researchers hope to optimize the design of electrode structure to minimize the above problems. Wang et al. successfully prepared the $Co(OH)_2$@CW cathode by depositing $Co(OH)_2$ on graded porous CW.[78] The top surface of the CW and inside its channels are covered by a thin, compact, uniform coating of $Co(OH)_2$ nanoflakes (Figures 8A–8C). C, O, and Co elements are evenly distributed in the observation area, implying a successful and uniform deposition of the Co $(OH)_2$@CW (Figures 8D–8F). The porous and flowerlike structure of $Co(OH)_2$ makes the close interface between CW and $Co(OH)_2$, which promotes the improvement of the electrochemical performances.[79,80] In this study, a hierarchically porous CW was used as the anode, cellulose paper as the separator and $Co(OH)_2$@CW as the cathode; a low-cost, green, and sustainable all-solid-state ASC was fabricated, as shown in Figure 8G. The all-solid-state ASC exhibited excellent capacitance retention, retaining 85% of the initial value after 10,000 GCD cycles, and powered an LED (2.5 V, 1.0 W) for 30 min by two in series (Figure 8I). It demonstrated impressive high capacitance of 2.2 F cm^{-2} and 34.8 F g^{-1} at the current density of 1.0 mA cm^{-2}(Figure 8H). These results are much better than those of most carbon-based and metal oxides–based SCs reported recently (Figures 8J and 8K). In conclusion, promising energy storage devices with good electrochemical performance can be made by combining metal oxides/hydroxides with wood material. The data obtained may also provide new research ideas on device structure design for electrochemical energy storage.

Developing favorable electrode materials is an effective way to improve the storage capacity of capacitors and to achieve high performance of super-capacitors.[81] In addition to the common electrode materials discussed above, studies have been carried out to produce new composite electrode materials by combining the above electrode materials. Zhang et al. prepared conductive porous wood carbon (PWC) by pyrolysis of natural balsa wood, and then the PWC/MnO_2/GQDs electrode was prepared by hydrothermal treatment and electrodeposition, which made MnO_2 and graphene quantum dots grow *in situ* on porous wood carbon, Figure 9A shows

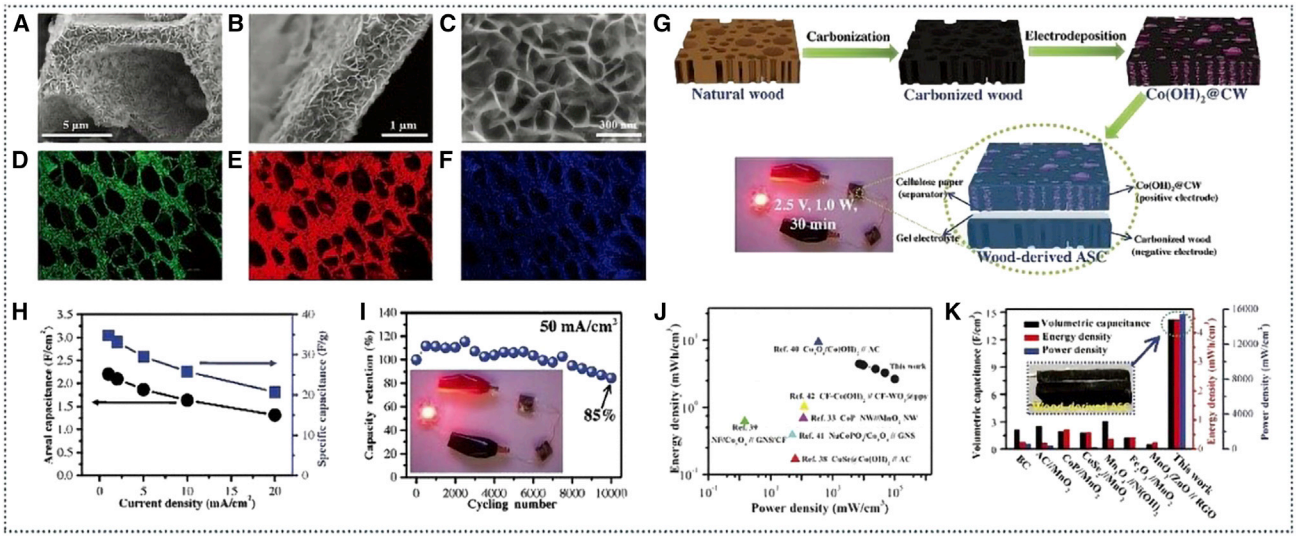

Figure 8. Microstructure and properties of materials

(A–C) Top view of the CW@Co(OH)$_2$, showing the Co (OH)$_2$ nanoflakes homogeneously intimate grown on the CW and inside its channel.

(D–F) Elemental mapping images of (D) C, (E) O, and (F).

(G) Fabrication of a wood-derived all-solid-state ASC.

(H) Rate performances based on the GCD curves at different current density.

(I) The ASC device measured at 50 mA cm^{-2} for 10,000 cycles, and the inset graph is an LED (2.5 V, 1.0 W) powered by the two in series.

(J,K) Energy/power density and volumetric capacitance of the wood-derived ASC compared with the previously reported electrode materials. Reproduced with permission.[78] Copyright 2018, John Wiley & Sons.

the preparation of the PWC/MnO$_2$ and PWC/MnO$_2$/GQDs electrodes.[82] The PWC/MnO$_2$ /GQDs electrode showed excellent electrochemical performance (Figure 9B). The area-specific capacitance is 2,712mF cm^{-2}, and the high corresponding mass specific capacitances based on mass are 188.4 F g^{-1} (Figure 9C); an internal resistance (Rs) value is 5.72 Ω, and the charge transfer resistance (Rct) value is 0.4 Ω (Figure 9F), showing the electrode has lower resistance and faster electron transfer. It also showed good long-term cycle stability, retaining approximately 95.3% after 2 000 cycles (Figure 9G). This is mainly due to a unique needlelike nanostructure formed on the surface and inside the PWC after adding GQDs (Figures 9D and 9E), which dramatically accelerated the ion diffusion and electron transport to stimulate the complete redox reactions.[83] This work provides a new perspective for the design of high-performance electrochemical–energy storage devices.

The metal sulfides have the potential to be used as high-performance electrode materials for supercapacitors. Among them, flowerlike CoS not only inherits the excellent properties of metal sulfide, but its special flowerlike structure also increases the effective contact area with electrolyte ions and enables better transport of electrolyte ions. Therefore, this flowerlike structure of CoS has received a considerable amount of interest.[84,85] As shown in Figure 10A, Xiong et al. has fabricated a novel carbonization lignin-free wood (CLFW) @Co-CoS hybrid electrode by a combination of vacuum filtration and carbonization.[86] It can be seen clearly that the CLFW@Co-CoS hybrid possesses better cycle stability than that of the CLFW@Co hybrid after experiencing 3,000 cycles at a scan rate of 100 mV s^{-1} (Figure 10C). This is mainly attributed to the cross-linked network formed from the CoS nanoflowers, which helps to stabilize the CLFW and Co nanoparticles. At a high scan rate of 200 mV s^{-1}, the CLFW@Co-CoS hybrid still shows a high capacitance retention of 95% (Figure 10D); it can be found that when the current density increased from 1 to 10 A g^{-1}, the gravimetric specific capacitance increased from 800 to 600 F g^{-1} and

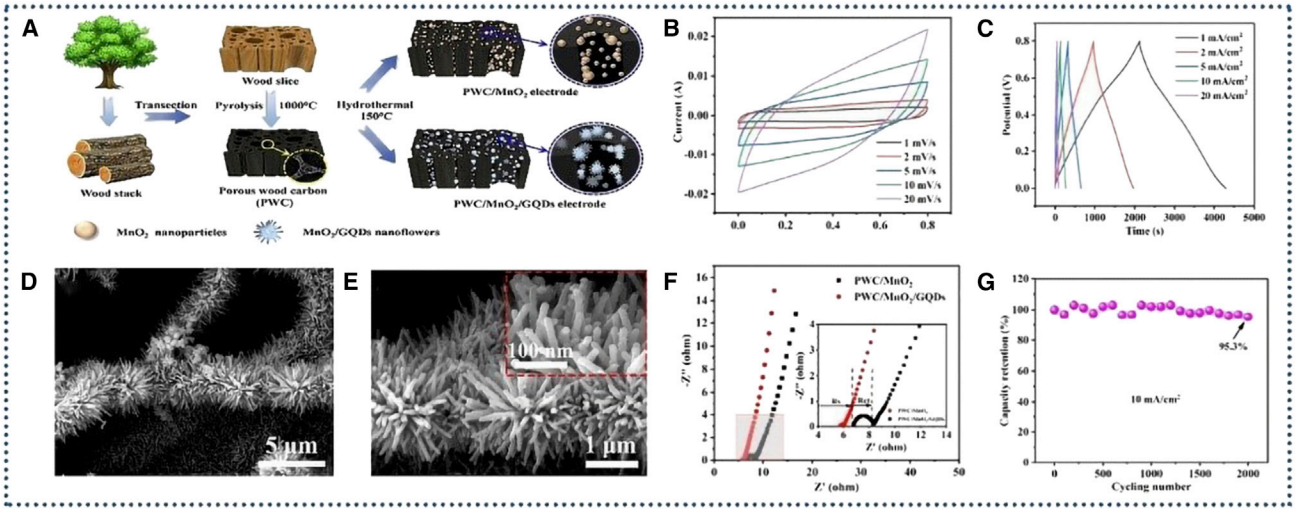

Figure 9. Preparation technology and properties of materials

(A) Schematic of the synthesis of the PWC/MnO_2 and PWC/MnO_2/GQDs electrodes.

(B) CV curves at various scan rates.

(C) GCD curves at different current densities.

(D) SEM images of PWC/MnO_2/GQDs15mg.

(E) Enlarged view of (D).

(F) Impedance curve of PWC/MnO_2 and PWC/MnO_2/GQDs15mg electrodes.

(G) Cycling performance of PWC/MnO_2/GQDs15mg. Reproduced with permission.[82] Copyright 2020, Elsevier.

the areal specific capacitance increased from 6 to 4 F cm^{-2} (Figure 10E). These specific capacitance values are much higher than those of the CLFW@Co hybrid and those reported in most previous work.[87–89] The CLFW@Co-CoS hybrid presents a high areal energy density of 610 μWh cm^{-2}, while at the same time maintaining a high areal power density of 192 mW cm^{-2}.

In addition, nickel sulfide (NiS) nanofiber with flowerlike structure not only has high specific capacitance, but also provides more transfer paths and diffusion channels for electron transfer and ion diffusion because of its novel nanosheet structure, which showed good rate performance and has received strong interest.[91–93] As shown in Figure 10B, Xiong et al. added vitrimer to CW as a reinforcing and molding agent and made a smart CLFW@Ni-NiS/vitrimer(V) composite multifunctional material with good reshaping, shape-memory, and self-healing properties.[90] The resultant CLFW@Ni-NiS/V hybrid assembled a symmetric SC, exhibited excellent electrochemical performance (Figures 10F and 10G). It not only shows high gravimetric, areal, and volumetric energy densities of 38Wh kg^{-1}, 687 μWh cm^{-2} and 58Wh L^{-1}, but also simultaneously maintains high power densities of 56 kW kg^{-1}, 202 mW cm^{-2} and 39 kW L^{-1}, and greatly enhances the cycle stability of wood-based materials.

APPLICATION OF WOOD IN BATTERY

Wood-based sodium metal battery

The demands for large-scale and low-cost energy storage technologies for transportation electrification and renewable energy storage are rapidly emerging worldwide.[94–98] Sodium metal anodes have attracted significant attention due to their high specific capacity, low redox potential and abundant resources.[99] It opens up new opportunities for developing next-generation rechargeable batteries with both high-power and high-energy densities.[100] One of the remaining major

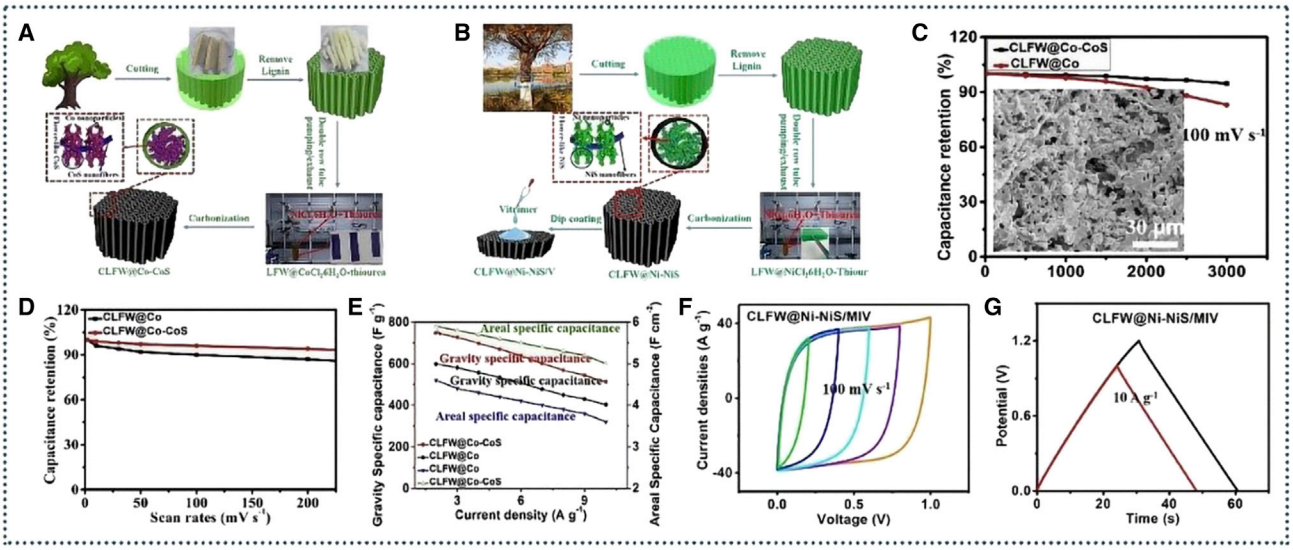

Figure 10. Preparation technology and properties of materials

(A) Displays the fabrication procedure of the CLFW@Co-CoS hybrid. Reproduced with permission.[86] Copyright 2020, Elsevier BV.

(B) Presents the fabrication procedure of the CLFW@Ni-NiS/V hybrid. Reproduced with permission.[90] Copyright 2020, Royal Society of Chemistry.

(C) The cycle stability of the CLFW@Co and CLFW@Co-CoS hybrid at a scan rate of 100 mV s^{-1} after experiencing 3000 cycles, the inset presented shows the SEM image of the CLFW@Co-CoS hybrid microstructure after cycling test.

(D) The change of capacitance retention of the CLFW@Co and CLFW@Co-CoS hybrid with the increase of scan rates.

(E) The gravimetric specific capacitance and area specific capacitance of the CLFW@Co and CLFW@Co-CoS hybrid under various current densities. Reproduced with permission.[86] Copyright 2020, Elsevier BV.

(F) The comparison of the (F) CV curves at a scan rate of 100 mV s^{-1}.

(G) GCD curves at a current of 10 A g^{-1} of the CLFW@Ni-NiS/MIV hybrid. Reproduced with permission.[90] Copyright 2020, Royal Society of Chemistry.

challenges now for sodium-ion batteries (SIBs) is to find a low-cost, high-performance anode material. Among various anode candidates,[101] hard carbon is still one of the most promising candidates due to its potentially low cost, scalability, and long-cycling performance.[102–105] Shen et al. have successfully demonstrated an ultra-thick, low-tortuosity, and mesoporous carbon directly from natural abundant wood by a simple carbonization process, which functions as an excellent binder-free, current collector-free anode in SIBs.[106] It was found that numerous mesopores are also observed on the wall of the wood carbon (Figure 11A and 11B). The size of these mesopores is under 100 nm, which indicates a short diffusion length for Na ions into the wood carbon wall during electrochemcial sodiation/desodiation. Benefiting from the unique construction, an ultrathick wood carbon anode (850 μm) with a large mass loading (55 mg cm^{-2}) can deliver a high areal capacity of 13.6 mA h cm^{-2}, much higher than traditional LIB areal capacity (≈3.5 mA h cm^{-2} for graphite) (Figure 11C). Excellent cycling performance in full cells with $Na_3V_2(PO4)_3$ cathodes was also demonstrated. Zheng et al. obtained a low-cost, biomass-derived hard carbon that can be used as an anode material by one-step pyrolysis with poplar as a raw material.[107] It can provide a high specific capacity of 330mAh/g and an initial Coulombic efficiency of 88.3% in half cells (Figures 11D–11G). A SIB full-cell architecture with this hard carbon anode delivers a specific energy of 212.9 Wh/kg(The anode-active + The cathode-active) at 1C, with 71% of the initial discharge capacity retained after 1200 cycles at 5C (Figure 11H). With an industrial-level mass loading (20.5 mg/cm2for the cathode), getting a capacity fade of only 6% within 600 cycles at 2C, and the capacity could recover nearly completely by setting the current rate to C/10 after 1,400 cycles, indicating the active electrode materials barely degraded (Figure 11I).

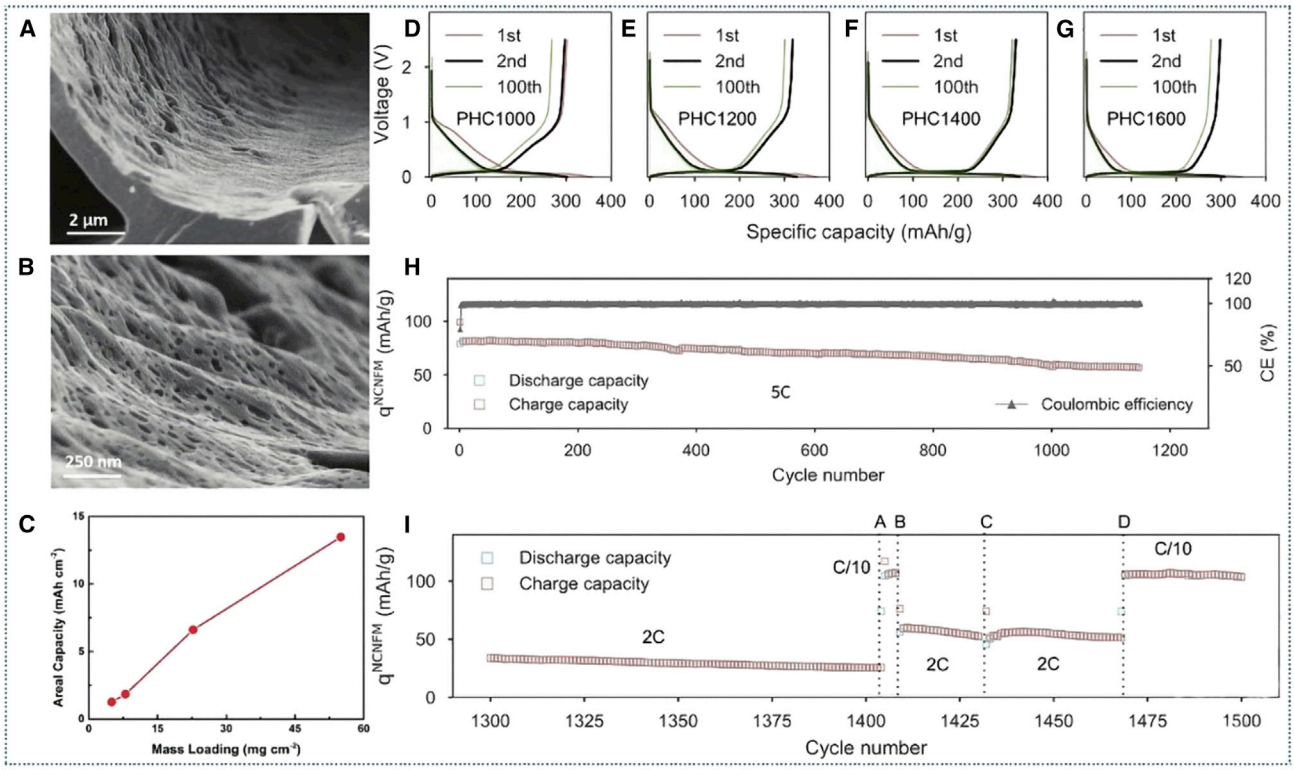

Figure 11. Study on the application of wood in SIBs

(A and B) Top-viewed SEM images of wood slabs after carbonization, (A) parallel; (B) enlarged of (A).

(C) Areal capacities achieved at different mass loadings. Reproduced with permission.[102] Copyright 2016, Wiley-VCH Verlag.

(D–G) Charge/Discharge profiles of the half-cells of (D) PHC1000, (E) PHC1200, (F) PHC1400, (G) PHC1600.

(H) The long-term cycling performance at 5C.

(I) Primarily decay analyzing. Reproduced with permission.[107] Copyright 2019, Elsevier BV.

Wood-based lithium battery

Lithium (Li) metal anode is considered as "the Holy Grail" of the next generation of energy storage systems because of its high theoretical specific capacity (3,860 mAh g^{-1}) and low electrochemical potential (- 3.04 V versus the standard hydrogen electrode).[108–110] However, there are some problems with the Li metal anode, such as amorphous growth of lithium dendrite,[111] electrolyte consumption, low coulomb efficiency due to continuous reaction with electrolyte,[112] and solid electrolyte interface (SEI) film fracture due to volume expansion,[113] which resulted in short cycle life and safety issues; hence, the practical application of Li metal batteries is greatly limited. In order to solve these problems, researchers have tried to use the natural 3D porous structure of wood to inhibit the growth of lithium dendrite, so as to improve the cycling stability of Li metal anode. Table 2 gives a comparison of some key parameters of various wood-based battery materials. For example, Yang et al. Introduced a facile synthesis method of MnO/C nanocomposites material.[114] Using the MnO/C nanocomposite material as the anode of a Li-ion battery, after 100 cycles of charge-discharge treatment, the MnO/C nanocomposite material could still keep a high reversible charge capacity of 952 mAh g^{-1}, showing its excellent cycle stability. The Coulombic efficiency steadily reached about 99% as the cycle number increased. Zhang et al. prepared a Li/C-wood electrode with high-capacity and low-curvature by injecting metal Li into CW channels,[115] as shown in Figure 12A. The wettability between C-wood and Li metal is critical. To make the surface of CW

Table 2. Summary of key parameters of various wood-based materials for battery

Ref.	Wood species	Electrode	Treatment condition	Surface area[m^2 g^{-1}]	Active mass loading [mg cm^{-2}]	Electrochemical performance	Electrolyte
48	Bass wood	TARC	N_2 (950°C, 2h); NH_3 activation	1438	–	241 mW cm^{-2} at 330 mA cm^{-2}; 945.2 Wh kg_{Zn}^{-1} at 10 mA cm^{-2}; over 100 h after 4 mechanical charges	KOH (6M)
106	Hard wood	CW	Air (260°C,8h); Ar (1000°C,2h)	–	55	areal capacity of 13.6 mA h cm^{-2}	NaClO (1M)
107	Poplar wood	CW	Ar (1400°C,2h)	–	7	330 mAh/g; initial Coulombic efficiency of 88.3%	–
115	Bass wood	Li/C-wood	Ar (1000°C, 6 h)	–	11 wt%, (28mg cm^{-2})	90 mV at 3 mA cm^{-2};150 h at 3 mA cm^{-2}	–
120	Balsa wood	CNT/Ru-coated F-Wood	chemical delignification	–	–	0.85 V at 100 mA g^{-1};220 cycles	LiTFSI / TEGDME (1 M)
130	Alsa wood	–	chemical delignification	–	–	over 200 cycles; capacity of 1000 mAh g^{-1};low overpotential of 1.5 V	lithium bis (trifluoromethane) sulfonimide (1 M)
134	Bass wood	3D-wood	(1000°C, 6h)	216.77	–	91.77% at 10mA cm^{-2}; energy efficiency is 75.44%	0.1 M $VOSO_4$+ 3 M H_2SO_4

more lithium friendly, they coated the channel walls of C-wood with a thin layer of ZnO. Molten Li was fast flooded into the channels of ZnO-coated C-wood, and the shiny Li/C-wood composite was formed (Figure 12B and 12D). Such a fast process is mainly attributed to the favorable reaction between Li metal and ZnO and the capillary force on lithiophilic surface as driving force. In symmetrical cells, the electrode presents a lower overpotential (90 mV at 3 mA cm^{-2}), more-stable stripping/plating profiles, and better cycling performance (150h at 3 mA cm^{-2}) compared to a bare Li metal electrode. Thus, this study provides a new idea for making stable Li metal anode, as well as a broader prospect for the application of high-energy-density Li metal batteries.

Lithium-oxygen batteries (LOBs) are used as a new type of energy storage battery; the positive active material is oxygen and the negative electrode is the lithium sheet with very low electrode potential and theoretically high specific capacity.[117] LOBs have attracted extensive attention for its ultrahigh energy density (ca. 3460 Wh kg^{-1}), which is several times larger than that of state-of-the-art Li-ion batteries.[118] However, the slow kinetics of ORR and oxygen evolution reactions (OER) on an oxygen electrode lead to low energy density and energy efficiency, which seriously hinders its practical application.[119,120] Therefore, it is important to find a cathode structure which is conducive to oxygen diffusion as well as to lithium ion and electronic transport so that the electrochemical performance of LOBs can be improved.

Wood is a 3D multichannel structure composed of cavity tube and provides favorable support for multiphase transportation. Chen et al. converted a rigid and electrically insulating wood membrane into a flexible and electrically conductive material for electron transmission through simple chemical delignification and CNT/ruthenium (Ru) coating process;[116] the resulting cell walls are comprised of cellulose nanofibers with abundant nanopores, which are ideal for Li^+ ion transport, whereas the unperturbed wood lumina act as a pathway for O_2 gas transport. Thus, a continuous three-channel flexible wood-based cathode was constructed. Figure 12C illustrates the breathable triphase redox reaction process involving electrons, Li^+ ions, and O_2 gas, and their transport in the F-Wood-based cell. The overpotential of the CNT /Ru-coated F-Wood cathode at a low current density of 100 mA g^{-1} is only 0.85 V (corresponding to a round-trip efficiency of ≈82%) (Figure 12E). The noncompetitive triple pathway

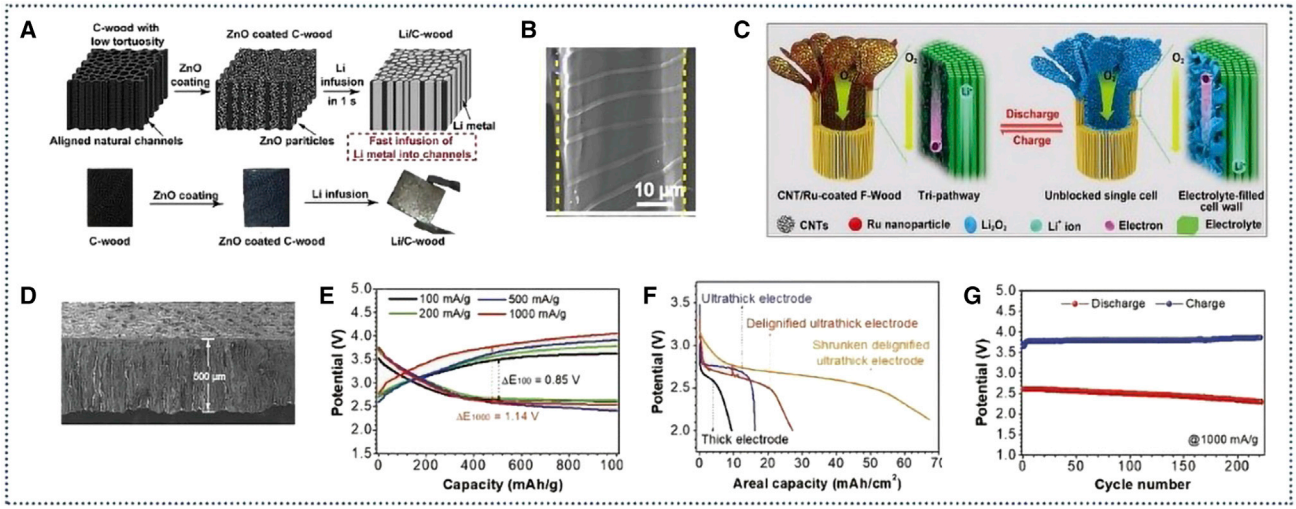

Figure 12. Preparation technology and properties of materials

(A) Fabrication process of the Li/C-wood composite.

(B) Cross sectional SEM images of C-wood present typical channel structure. Reproduced with permission.[115] Copyright 2017, National Academy of Sciences.

(C) Schematic illustrations of the breathable lithium storage in the electrode. Reproduced with permission.[116] Copyright 2019, Wiley-VCH Verlag.

(D) Cross sectional SEM images of Li infusion in the channel void space. Reproduced with permission.[115] Copyright 2017, National Academy of Sciences.

(E) Charge-discharge profiles at various current densities of 100, 200, 500, and 1,000 mA g^{-1}.

(F) Discharge curves of the initial cycle for the CNT/Ru-coated F-Wood electrodes with moderate thickness (≈0.5 mm, thick electrode), large thickness (≈1.8 mm, ultrathick electrode), large thickness and complete delignification treatment (complete delignified ultrathick structure), and the shrunken delignified ultrathick electrode.

(G) Average charge-discharge potentials of the initial 220 cycles at 1,000 mA g^{-1}. Reproduced with permission.[116] Copyright 2019, Wiley-VCH Verlag.

design endows the wood-based cathode with a low overpotential of 0.85 V at 100 mA g^{-1}, a record-high areal capacity of 67.2 mAh cm^{-2}(Figure 12F), a long cycling life of 220 cycles (Figure 12G), and superior electrochemical and mechanical stability. This work proves that the unique three channel structure of wood can enable noncompetitive transportation of O_2, Li^+ and electronics, solve the problem of slow chemical reaction kinetics of traditional LOBs, and find a balance between the electrochemical performance and mechanical flexibility of energy storage devices, thus establishing a promising pathway for sustainable development of wearable and portable energy storage devices in the future.

With ongoing rapid industrial development in the world, carbon dioxide (CO_2) emission has also been increasing over the years contributing to the global warming. Hence, reducing CO_2 emissions and making full and effective use of CO_2 have become one of the key tasks the world needs. The recent emergence of Li-CO_2 batteries with high energy density provides one possible solution for CO_2 conversion and utilization,[121] as they are regarded as promising electrochemical devices to simultaneously capture CO_2 and deliver electric energy.[122] With the help of redox chemical interaction between Li and CO_2, a Li-CO_2 battery is 6 times higher than the energy density (1876 Wh kg^{-1}) obtained by a Li ion battery.[123] However, in spite of these great merits, some problems remain such as low round-trip efficiency during cycling,[124] poor reversibility on recharge,[125] and so on. This has seriously impeded further development and practical applications of Li-CO_2 batteries.[126–128]

Xu et al. reported a high-capacity, mechanically flexible and highly rechargeable Li–CO_2 battery based on a flexible cathode.[129] The overpotential of the electrode

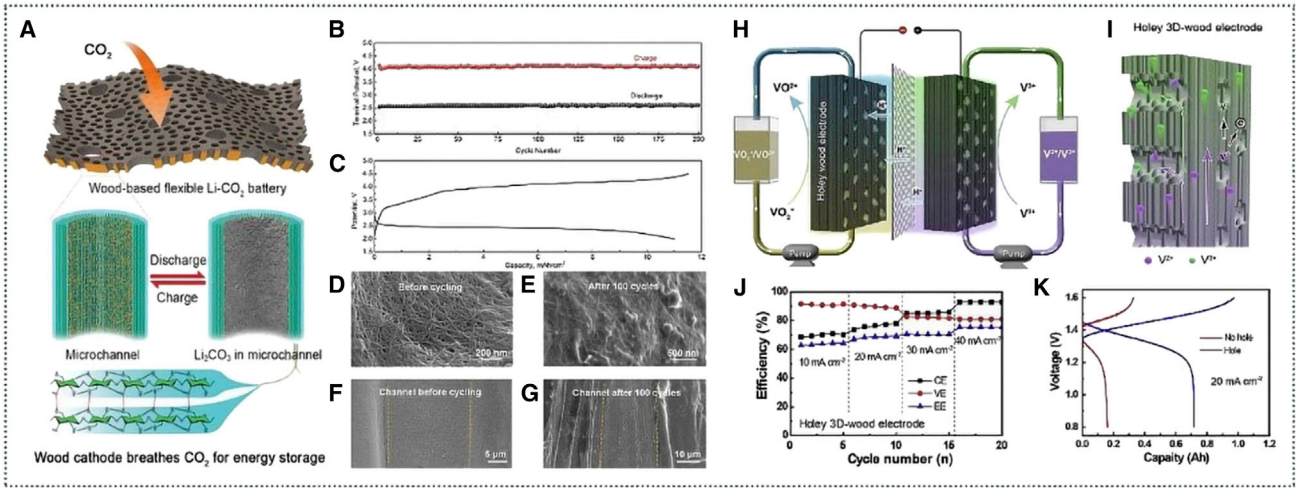

Figure 13. Performance and working principle of materials

(A) The schematic of the Li–CO_2 battery based on the flexible wood cathode absorbing CO_2 for energy storage.

(B) Terminal voltage of each charge (red) and discharge (black) showing almost no change over 200 cycles.

(C) Discharge-charge profile of the Li–CO_2battery with a 2mm thick cathode revealing the ultrahigh capacity of 11 mA h cm^{-2}.

(D) SEM image of the pristine cathode surface before cycling showing the CNT network on top.

(E) SEM image of the cathode surface after 100 cycles which has identical morphology to the pristine cathode.

(F) SEM image of microchannels in the pristine cathode without any obstructions for gas flow.

(G) SEM image of microchannels in the cathode after 100 cycles which preserves the unblocked pathways after cycling. Reproduced with permission.[129] Copyright 2018, Royal Society of Chemistry.

(H) Schematic detailing the working principles of the holey 3D-wood electrode for vanadium flow batteries.

(I) Enlarged holes on the 3D-wood electrode help enable mass transfer so that the vanadium cations can diffuse between the wood channels.

(J) The rate capability of the holey 3D-wood electrode as gauged by the CE, VE, and EE of the VFB.

(K) Galvanostatic charge-discharge curves of the VFB single cell with 3D-wood electrodes with and without holes at a current density of 20 mA cm^{-2}. Reproduced with permission.[130] Copyright 2020, Elsevier BV.

remained constant at 1.5 V throughout the 200 cycles, demonstrating the excellent and stable performance of the flexible wood-based cathode Li–CO_2 battery (Figure 13B); the architecture and surface morphology of the cathode remained identical even after long-term cycling—its pristine surfaces are preserved (Figures 13D–13G). Even the 2-mm-thick cathode showed an ultrahigh capacity of 11mAh cm^{-2} (Figure 13C). This shows that the channel structure of a wood-based cathode has facilitated excellent transport performance. The structure schematic is shown in Figure 13A. The wood-based cathode Li–CO_2 battery takes advantage of the natural microchannels (vessels and lumina) structure of wood to ensure sufficient gas flow of CO_2, and the nanochannels (gaps between the cellulose nanofibers) of the cell walls are filled with electrolyte. By placing a Ru-decorated CNT network on the interior walls of the microchannels, ample surface area is provided for the discharge product deposition. Thus, there is no transport barrier in this Li–CO_2 battery design, which ensures the excellent rechargeability of the system. It can be seen that the unique 3D channel structure of wood greatly stimulates the transportation of electrolyte and carbon dioxide gas. The excellent flexibility of the wood cathode due to the removal of lignin and hemicellulose by chemical treatment, enables the wood-based Li–CO_2 battery to process excellent electrochemical performance, which subsequently makes it a promising candidate for wearable energy storage devices in various applications.

Cellulose nanofibers (CNF) have highly enhanced dispersibility in various solvents, which can be processed into nanostructured porous materials. Thus, in addition to

the above applications, lignocellulose has also been investigated as lithium-ion battery separators. Hyeyun et al. prepared carboxylated cellulose nanofibers by TEMPO-mediated oxidation (TOCN), processed them into asymmetric mesoporous membranes by a facile paper-making approach, and studied as lithium ion battery diaphragms.[131] Its protonated counterpart (TOCN-COOH) showed highly improved electrochemical and cycling stability, displaying 94.5% of discharge capacity maintained after 100 cycles at 1 C rate of charging and discharging. Obviously, the wood-based TOCN-membranes have potential as an eco-friendly alternative to conventional fossil-fuel-derived separators without adverse side effects.

Wood-based vanadium redox battery

Due to the intermittency and unpredictability of renewable energy, there is an urgent demand for large-scale energy storage systems in today's society.[132–134] In addition to the Li batteries mentioned above in this article, the vanadium flow battery (VFB) is widely regarded as one of the most reliable large-scale energy storage technologies because of its flexible design, long cycle life, and high degree of safety. Jiao et al. prepared a low-cost, holey 3D-wood electrode for VFBs by a facile perforation and carbonization process.[130] Figures 13H and 13I presents the design of the holey 3D-wood electrode in the VFB, where the active vanadium cations are dissolved in the electrolyte and circulated between the electrolyte tanks and the holey 3D-wood electrodes by pumps. The 3D-wood electrode demonstrates a conductivity of 20 S cm^{-1}; The holey 3D-wood electrode demonstrates a high voltage efficiency of 91.77% at 10 mA cm^{-2}, which is 10.59% higher than the electrode without pore engineering (Figure 13J); the reduced polarization in the VFB with the holey 3D-wood electrode results in an increase in the discharge capacity from 0.16 to 0.72 Ah, a 4.5-fold improvement(Figure 13K); the energy efficiency of the holey 3D-wood electrode is measured to be 75.44% in the single cell, which shows a good workability .

APPLICATION OF WOOD IN CATALYTIC HYDROGEN EVOLUTION

As a green and efficient energy, hydrogen is expected to replace fossil fuels.[135] Hydrogen evolution reaction (HER) in electrochemical water splitting has attracted considerable interest. There are mainly two reasons: (1) hydrogen gas (H_2) produced in the process is a promising candidate as high-energy carrier for clean fuels; (2) the carbon-free emission strategy is facile and sustainable to efficiently resolve energy crisis and environmental deterioration.[136,137] Here we present some research on the application of wood as a support template in catalytic hydrogen evolution. Huang et al. developed a wood-derived carbon framework to support 3D conductive electrodes of Rhenium disulfide (ReS_2) nanosheets for direct electrocatalytic hydrogen production.[138] The preparation process of a wooden electrode is shown in Figure 14A. The overall size of the carbonized SW(CSW) is almost reduced to half of the original SW, and its color changed from yellow to carbon black. This is mainly due to the decomposition of cellulose and other organic components in SW, which were entirely converted to graphite carbon. After the Chemical vapor deposition (CVD) growth, the black CSW framework appeared light gray because of the covering with ReS_2. In a water electrolysis configuration, ReS_2/CSW was finally used as a working electrode without any binders for H_2 production (Figure 14B). From the micromorphology, we can find that the 3D porous skeleton structure remains after carbonization, and the surfaces of the porous skeleton are covered with high-density freestanding ReS_2 nanosheets after the CVD growth at 750°C(Figures 14C–14F). The ReS_2/C_{SW}-750 electrode exhibited the smallest over-potential of 260 mV versus RHE at a current density of 10 mA cm^{-2}(357mV

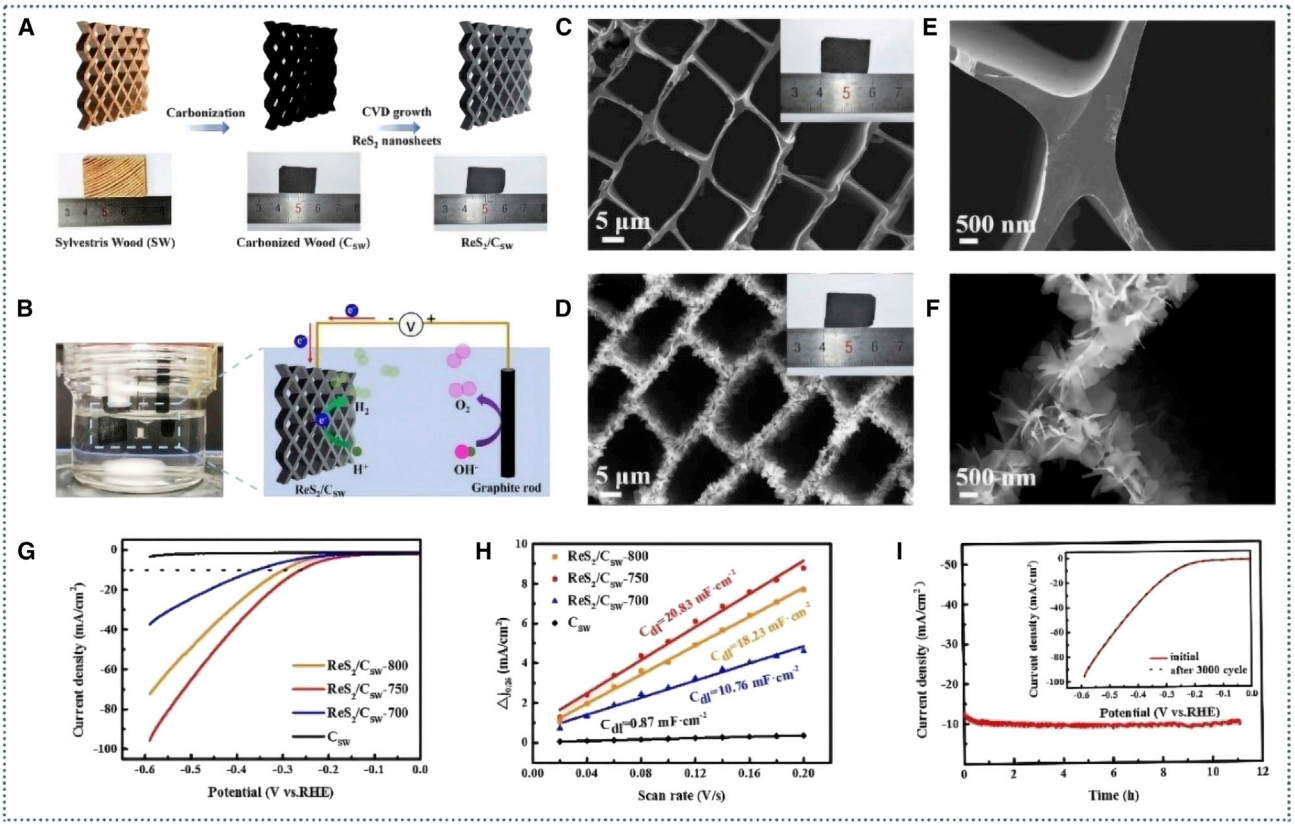

Figure 14. Microstructure and properties of materials

(A) Schematic illustration of the preparation procedures of wood-derived electrode with corresponding sample photographs.

(B) Experimental photograph and its schematic diagram of the electrode directly used for H_2 production in a water electrolysis configuration.

(C–F) Morphology characterizations of C_{SW} and ReS_2/C_{SW}-750. (C), (E) and (D), (F) Top-view SEM images of C_{SW} and ReS_2/C_{SW}-750 with low and high magnifications, respectively.

(G–I) Electrochemical characterizations of ReS_2/C_{SW} electrodes. (G) LSV polarization curves; (H) Linear fitting of the differences in current density at 0.26 V versus RHE plotted against scan rates for C_{dl}; (I) Stability test at −0.26 V versus RHE, and inset showing the polarization curves of ReS_2/C_{SW}-750 initial and after 3000 continuous CV cycles. Reproduced with permission.[138] Copyright 2021, Springer.

for ReS_2/C_{SW}-700 and 299mV for ReS_2/C_{SW}-800) (Figure 14G). The ReS_2/C_{SW}-750 electrode demonstrates the largest C_{dl} of 20.83 mF cm^{-2}. Consequently, the ECSA value of ReS_2/C_{SW}-750 electrode is estimated to be 521 cm^2_{ECSA} (Figure 14H), which suggests that the HER performance could be quite outstanding.[139] Also, the stability is over 11h (Figure 14I). It can be seen that wood-based composites show excellent HER performance. As such, carbon framework derived from natural wood is earth-abundant, ecofriendly, and renewable, and it can be potentially applied in the green energy industry.

CONCLUSION AND PROSPECT

In this paper, the latest research progress of wood-based energy storage materials in relation to the preparation and application of energy storage devices is reviewed, with emphasis on the application of wood in supercapacitor, battery, and catalytic hydrogen evolution. The preparation and modification methods (delignification, high-temperature carbonization, physical/chemical activation, etc.) in these studies not only endow wood with excellent electrical conductivity and provide a larger specific surface area for loading electroactive materials, but also open up new

possibilities for a variety of applications of energy storage devices based on natural wood. The wood, 3D, porous, straight-channel structure provides more space and channels for the storage and transmission of electrolyte ions, and its integrity has been preserved regardless of what kind of treatment was applied and without the use of polymer binder. This research work will provide additional information and help open up new possibilities for the construction and application of multifunctional renewable wood-based composites, and may inspire future development of electrochemically active materials from natural materials for a variety of renewable energy utilizations.

At present, more and more research is drawn toward wood-based energy storage devices and has since made some encouraging progress. However, some challenges remain as follows:

(1) Counter the brittleness and improve mechanical strength of CW. Although wood obtained excellent electrical conductivity after high temperature carbonization, the energy consumption in the preparation process is high. More concerning is that high temperature carbonization leads to pyrolysis of cellulose, hemicellulose, and other components in the wood, which subsequently cause brittleness and a significant decrease in the mechanical strength of the wood. This greatly limits the application of CW for energy storage. Also, CW is difficult to meet the energy storage requirements in different environments, especially compared with the performance development of flexible and foldable electronic devices. Therefore, we can improve the mechanical properties of materials by loading resin compounds. Perhaps we can also consider from the perspective of supercompressed wood, and select mild carbonization conditions to improve the mechanical properties of CW.
(2) Explore the relationship between the hierarchical porous structure and the electrochemical properties of wood. Investigating the influence of wood pore size on electrochemical performance, and design wood materials with adequate or optimal pore structure and size to achieve high quality load, so as to improve the energy density of materials; in order for active substances to enter the wood, ensure that the hole size of the wood cannot be too small. At the same time, make the electroactive material evenly distributed in the wood conduit to improve the electrochemical performance. The common treatment method is *in situ* growth, which can closely combine wood with active substances. In addition, broaden the applications of this design to suit other hybrid materials. Usually, we control the specific surface area of materials by controlling the time of physical/chemical activation to explore the electrochemical properties corresponding to the optimal pore size.
(3) The low density and too much pore space of wood-derived carbon provide a fast channel for the transmission of ions and electrons, but too large porosity is not conducive to improve the volumetric energy density and capacity of energy storage devices. Therefore, we can design the pore space of materials by activating or filling active substances, find the best volume energy density and energy, and determine the most appropriate pore space.
(4) Design simple, efficient, and green wood-based energy storage devices. Although some progress has been made in this area, more efforts are still needed to make wood-based energy storage devices with good electrochemical performance in a simple, efficient, and environmentally friendly way. We can choose environmentally friendly heteroatoms to further improve the electrochemical properties of materials, such as N, S, Mn and so on.

(5) Reduce production costs. Although we have chosen cheap wood as raw material, it is still the top priority to continue to develop suitable wood pretreatment solvent systems and recyclable catalysts, and to reduce the use of chemicals to reduce production costs! At the same time, the cost problem is also the key to promote the commercial development of wood-based energy–storage devices.

In conclusion, taking their inspiration from efficient ion transfer in wood due to its inherent anisotropic, 3D, porous structure, researchers found that wood is highly suitable for rapid mass transfer along the channel direction while maintaining mechanical consistency; therefore, it is an ideal choice for building high-performance energy storage devices. With increasing demand for advanced energy storage technology and equipment, the energy storage market is accordingly driven for products with higher performance, longer life, better safety, and environmental friendliness. Further research is needed to reduce energy use, reduce production cost, and protect the environment; and to improve energy density, cycle stability, and other energy storage characteristics. Wood has incomparable advantages as a material for energy storage devices. It is believed that further research could help to establish broad application prospects in the field of energy storage and conversion.

ACKNOWLEDGMENTS

This work was supported by the National Natural Science Foundation of China (31760186), the National Natural Science Foundation of China (32101455), and the Inner Mongolia Autonomous Region "grassland talents" innovative talent team project.

AUTHOR CONTRIBUTIONS

X.S. reviewed the literature and wrote the manuscript. J.W., X.Z., and L.W. contributed to literature collection. J.Y., Z.C., J.Y., and X.W. contributed to manuscript revision.

DECLARATION OF INTERESTS

The authors declare no competing interests.

REFERENCES

1. Zheng, S., Xue, H., and Pang, H. (2018). Supercapacitors based on metal coordination materials. Coord. Chem. Rev. *373*, 2–21. https://doi.org/10.1016/j.ccr.2017.07.002.

2. Liu, C., Yan, X., Hu, F., Gao, G., Wu, G., and Yang, X. (2018). Toward superior capacitive energy storage: Recent advances in pore engineering for dense electrodes. Adv. Mater. *30*, e1705713. https://doi.org/10.1002/adma.201705713.

3. Xu, W., Jiang, Z., Yang, Q., Huo, W., Javed, M.S., Li, Y., Huang, L., Gu, X., and Hu, C. (2018). Approaching the lithium-manganese oxides' energy storage limit with Li2MnO3 nanorods for high-performance supercapacitor. Nano Energy *43*, 168–176. https://doi.org/10.1016/j.nanoen.2017.10.046.

4. Wu, P., Cheng, S., Yang, L., Lin, Z., Gui, X., Ou, X., Zhou, J., Yao, M., Wang, M., Zhu, Y., and Liu, M. (2016). Synthesis and characterization of self-standing and hghly fexible δ-MnO2@CNTs/CNTs composite films for direct use of supercapacitor electrodes. ACS Appl. Mater. Interfaces *8*, 23721–23728. https://doi.org/10.1021/acsami.6b07161.

5. Bose, S., and Das, C. (2015). Sawdust: From wood waste to pore-former in the fabrication of ceramic membrane. Ceram. Int. *41*, 4070–4079. https://doi.org/10.1016/j.ceramint.2014.11.101.

6. Pan, J., Pan, J., Cheng, X., Yan, X., Lu, Q., and Zhang, C. (2014). Synthesis of hierarchical porous silicon oxycarbide ceramics from preceramic polymer and wood biomass composites. J. Eur. Ceram. Soc. *34*, 249–256. https://doi.org/10.1016/j.jeurceramsoc.2013.08.004.

7. Chen, C., Zhang, Y., Li, Y., Kuang, Y., Song, J., Luo, W., Wang, Y., Yao, Y., Pastel, G., Xie, J., and Hu, L. (2017). Highly conductive, lightweight, low-tortuosity carbon fameworks as ultrathick 3D current collectors. Adv. Energy Mater. *7*, 1700595. https://doi.org/10.1002/aenm.201700595.

8. Chen, C., Kuang, Y., Zhu, S., Burgert, I., Keplinger, T., Gong, A., Li, T., Berglund, L., Eichhorn, S.J., and Hu, L. (2020). Structure-property-function relationships of natural and engineered wood. Nat. Rev. Mater. *5*, 642–666. https://doi.org/10.1038/s41578-020-0195-z.

9. Lu, Y., Li, J., Zhang, Y., Zhong, G., Liu, B., and Wang, H. (2020). Wood-derived carbon functional materials. Prog. Chem. *32*, 906–916. https://doi.org/10.7536/pc191223.

10. Wu, C., Zhang, S., Wu, W., Xi, Z., Zhou, C., Wang, X., Deng, Y., Bai, Y., Liu, G., Zhang, X., et al. (2019). Carbon nanotubes grown on the inner wall of carbonized wood tracheids for high-performance supercapacitors. Carbon

150, 311–318. https://doi.org/10.1016/j.carbon.2019.05.032.

11. Urbain, F., Smirnov, V., Becker, J.-P., Lambertz, A., Yang, F., Ziegler, J., Kaiser, B., Jaegermann, W., Rau, U., and Finger, F. (2016). Multijunction Si photocathodes with tunable photovoltages from 2.0 V to 2.8 V for light induced water splitting. Energy Environ. Sci. 9, 145–154. https://doi.org/10.1039/c5ee02393a.

12. Yaddanapudi, H.S., Tian, K., Teng, S., and Tiwari, A. (2016). Facile preparation of nickel/carbonized wood nanocomposite for environmentally friendly supercapacitor electrodes. Sci. Rep. 6, 33659. https://doi.org/10.1038/srep33659.

13. Song, H., Xu, S., Li, Y., Dai, J., Gong, A., Zhu, M., Zhu, C., Chen, C., Chen, Y., Yao, Y., et al. (2018). Hierarchically porous, ultrathick, "breathable" wood-derived cathode for lithium-oxygen batteries. Adv. Energy Mater. 8, 1701203. https://doi.org/10.1002/aenm.201701203.

14. Lu, L.-L., Lu, Y.-Y., Xiao, Z.-J., Zhang, T.-W., Zhou, F., Ma, T., Ni, Y., Yao, H.-B., Yu, S.-H., and Cui, Y. (2018). Wood-inspired high-performance ultrathick bulk battery electrodes. Adv. Mater. 30, e1706745. https://doi.org/10.1002/adma.201706745.

15. Han, L., Wang, J., Mu, X., Liao, C., Cai, W., Zhao, Z., Kan, Y., Xing, W., and Hu, Y. (2020). Anisotropic, low-tortuosity and ultra-thick red P@C-Wood electrodes for sodium-ion batteries. Nanoscale 12, 14642–14650. https://doi.org/10.1039/d0nr03059g.

16. Li, Y., Fu, K.K., Chen, C., Luo, W., Gao, T., Xu, S., Dai, J., Pastel, G., Wang, Y., Liu, B., et al. (2017). Enabling high-areal-capacity lithium-sulfur batteries: Designing anisotropic and low-tortuosity porous architectures. ACS Nano 11, 4801–4807. https://doi.org/10.1021/acsnano.7b01172.

17. Zhu, M., Li, Y., Chen, F., Zhu, X., Dai, J., Li, Y., Yang, Z., Yan, X., Song, J., Wang, Y., et al. (2018). Plasmonic wood for high-efficiency solar steam generation. Adv. Energy Mater. 8, 1701028. https://doi.org/10.1002/aenm.201701028.

18. Chen, F., Gong, A.S., Zhu, M., Chen, G., Lacey, S.D., Jiang, F., Li, Y., Wang, Y., Dai, J., Yao, Y., et al. (2017). Mesoporous, three-dimensional wood membrane decorated with nanoparticles for highly efficient water treatment. ACS Nano 11, 4275–4282. https://doi.org/10.1021/acsnano.7b01350.

19. Che, W., Xiao, Z., Wang, Z., Li, J., Wang, H., Wang, Y., and Xie, Y. (2019). Wood-based mesoporous filter decorated with silver nanoparticles for water purification. ACS Sustain. Chem. Eng. 7, 5134–5141. https://doi.org/10.1021/acssuschemeng.8b06001.

20. Bresser, D., Passerini, S., and Scrosati, B. (2013). Recent progress and remaining challenges in sulfur-based lithium secondary batteries–a review. Chem. Commun. (Camb.) 49, 10545–10562. https://doi.org/10.1039/c3cc46131a.

21. Song, J., Chen, C., Zhu, S., Zhu, M., Dai, J., Ray, U., Li, Y., Kuang, Y., Li, Y., Quispe, N., et al. (2018). Processing bulk natural wood into a high-performance structural material. Nature 554, 224–228. https://doi.org/10.1038/nature25476.

22. Zhu, M., Song, J., Li, T., Gong, A., Wang, Y., Dai, J., Yao, Y., Luo, W., Henderson, D., and Hu, L. (2016). Highly anisotropic, highly transparent wood composites. Advanced Materials 28, 5181–5187. https://doi.org/10.1002/adma.201600427.

23. Xia, Q., Chen, C., Li, T., He, S., Gao, J., Wang, X., and Hu, L. (2021). Solar-assisted fabrication of large-scale, patternable transparent wood. Sci. Adv. 7, eabd7342. https://doi.org/10.1126/sciadv.abd7342.

24. Chao, W., Wang, S., Li, Y., Cao, G., Zhao, Y., Sun, X., Wang, C., and Ho, S.-H. (2020). Natural sponge-like wood-derived aerogel for solar-assisted adsorption and recovery of high-viscous crude oil. Chem. Eng. J. 400, 125865. https://doi.org/10.1016/j.cej.2020.125865.

25. Yaddanapudi, H.S., Hickerson, N., Saini, S., and Tiwari, A. (2017). Fabrication and characterization of transparent wood for next generation smart building applications. Vacuum 146, 649–654. https://doi.org/10.1016/j.vacuum.2017.01.016.

26. Li, Y., Fu, Q., Yang, X., and Berglund, L. (2018). Transparent wood for functional and structural applications. Philos. Trans.- Royal Soc., Math. Phys. Eng. Sci. 376, 20170182. https://doi.org/10.1098/rsta.2017.0182.

27. Yorur, H., Kurt, S., and Yumrutas, H.I. (2014). The Effect of Aging on Various Physical and Mechanical Properties of Scotch Pine Wood Used in Construction of Historical Safranbolu Houses. Drv. Ind. 65, 191–196.

28. Pikul, J.H., Özerinç, S., Liu, B., Zhang, R., Braun, P.V., Deshpande, V.S., and King, W.P. (2019). High strength metallic wood from nanostructured nickel inverse opal materials. Sci. Rep. 9, 719. https://doi.org/10.1038/s41598-018-36901-3.

29. Zhu, M., Li, T., Davis, C.S., Yao, Y., Dai, J., Wang, Y., AlQatari, F., Gilman, J.W., and Hu, L. (2016). Transparent and haze wood composites for highly efficient broadband light management in solar cells. Nano Energy 26, 332–339. https://doi.org/10.1016/j.nanoen.2016.05.020.

30. Li, T., Zhu, M., Yang, Z., Song, J., Dai, J., Yao, Y., Luo, W., Pastel, G., Yang, B., and Hu, L. (2016). Wood composite as an energy efficient building material: Guided sunlight transmittance and effective thermal insulation. Adv. Energy Mater. 6, 1601122. https://doi.org/10.1002/aenm.201601122.

31. Chen, C., and Hu, L. (2018). Nanocellulose toward advanced energy storage devices: Structure and electrochemistry. Acc. Chem. Res. 51, 3154–3165. https://doi.org/10.1021/acs.accounts.8b00391.

32. Song, J., Chen, C., Wang, C., Kuang, Y., Li, Y., Jiang, F., Li, Y., Hitz, E., Zhang, Y., Liu, B., et al. (2017). Superflexible wood. ACS Appl. Mater. Interfaces 9, 23520–23527. https://doi.org/10.1021/acsami.7b06529.

33. Chen, C.J., Song, J.W., Zhu, S.Z., Li, Y.J., Kuang, Y.D., Wan, J.Y., Kirsch, D., Xu, L.S., Wang, Y.B., Gao, T.T., et al. (2018). Scalable and sustainable approach toward highly compressible, anisotropic, lamellar carbon sponge. Chem 4, 544–554. https://doi.org/10.1016/j.chempr.2017.12.028.

34. Muzaffar, A., Ahamed, M.B., Deshmukh, K., and Thirumalai, J. (2019). A review on recent advances in hybrid supercapacitors: Design, fabrication and applications. Renew. Sustain. Energy Rev. 101, 123–145. https://doi.org/10.1016/j.rser.2018.10.026.

35. Zhu, Y., Huang, H., Zhou, W., Li, G., Liang, X., Guo, J., and Tang, S. (2017). Low temperature reduction of graphene oxide film by ammonia solution and its application for high-performance supercapacitors. J. Mater. Sci. Mater. Electron. 28, 10098–10105. https://doi.org/10.1007/s10854-017-6771-3.

36. Chmiola, J., Yushin, G., Gogotsi, Y., Portet, C., Simon, P., and Taberna, P.L. (2006). Anomalous increase in carbon capacitance at pore sizes less than 1 nanometer. Science 313, 1760–1763. https://doi.org/10.1126/science.1132195.

37. Jin, Z., Yan, X., Yu, Y., and Zhao, G. (2014). Sustainable activated carbon fibers from liquefied wood with controllable porosity for high-performance supercapacitors. J. Mater. Chem. A Mater. Energy Sustain. 2, 11706–11715. https://doi.org/10.1039/c4ta01413h.

38. Ruiz, V., Blanco, C., Santamaria, R., Ramos-Fernandez, J.M., Martinez-Escandell, M., Sepulveda-Escribano, A., and Rodriguez-Reinoso, F. (2009). An activated carbon monolith as an electrode material for supercapacitors. Carbon 47, 195–200. https://doi.org/10.1016/j.carbon.2008.09.048.

39. Teng, S., Siegel, G., Wang, W., and Tiwariz, A. (2014). Carbonized wood for supercapacitor electrodes. Ecs Solid State Letters 3, M25-M28. https://doi.org/10.1149/2.005405ssl.

40. Liu, M.-C., Kong, L.-B., Zhang, P., Luo, Y.-C., and Kang, L. (2012). Porous wood carbon monolith for high-performance supercapacitors. Electrochim. Acta 60, 443–448. https://doi.org/10.1016/j.electacta.2011.11.100.

41. Zhang, W., Liu, T., Mou, J., Huang, J., and Liu, M. (2020). Ultra-thick electrodes based on activated wood-carbon towards high-performance quasi-solid-state supercapacitors. Phys. Chem. Chem. Phys. 22, 2073–2080. https://doi.org/10.1039/c9cp06181a.

42. Hu, C., and Dai, L. (2017). Multifunctional carbon-based metal-free electrocatalysts for simultaneous oxygen reduction, oxygen evolution, and hydrogen evolution. Adv. Mater. 29, 1604942. https://doi.org/10.1002/adma.201604942.

43. Pei, Z., Li, H., Huang, Y., Xue, Q., Huang, Y., Zhu, M., Wang, Z., and Zhi, C. (2017). Texturing in situ: N, S-enriched hierarchically porous carbon as a highly active reversible oxygen electrocatalyst. Energy Environ. Sci. 10, 742–749. https://doi.org/10.1039/c6ee03265f.

44. Shang, L., Yu, H., Huang, X., Bian, T., Shi, R., Zhao, Y., Waterhouse, G.I.N., Wu, L.-Z., Tung, C.-H., and Zhang, T. (2016). Well-dispersed

ZIF-derived Co,N-Co-doped carbon nanoframes through mesoporous-silica-protected calcination as efficient oxygen reduction electrocatalysts. Adv. Mater. *28*, 1668–1674. https://doi.org/10.1002/adma.201505045.

45. Shinde, S.S., Lee, C.-H., Sami, A., Kim, D.-H., Lee, S.-U., and Lee, J.-H. (2017). Scalable 3-D carbon nitride sponge as an efficient metal-free bifunctional oxygen electrocatalyst for rechargeable Zn-air batteries. ACS Nano *11*, 347–357. https://doi.org/10.1021/acsnano.6b05914.

46. Xu, J., Tan, Z., Zeng, W., Chen, G., Wu, S., Zhao, Y., Ni, K., Tao, Z., Ikram, M., Ji, H., and Zhu, Y. (2016). A hierarchical carbon derived from sponge-templated activation of graphene oxide for high-performance supercapacitor electrodes. Adv. Mater *28*, 5222–5228. https://doi.org/10.1002/adma.201600586.

47. Liang, H.-W., Zhuang, X., Brüller, S., Feng, X., and Müllen, K. (2014). Hierarchically porous carbons with optimized nitrogen doping as highly active electrocatalysts for oxygen reduction. Nat. Commun. *5*, 4973. https://doi.org/10.1038/ncomms5973.

48. Tang, Z., Pei, Z., Wang, Z., Li, H., Zeng, J., Ruan, Z., Huang, Y., Zhu, M., Xue, Q., Yu, J., and Zhi, C. (2018). Highly anisotropic, multichannel wood carbon with optimized heteroatom doping for supercapacitor and oxygen reduction reaction. Carbon *130*, 532–543. https://doi.org/10.1016/j.carbon.2018.01.055.

49. Lv, S., Fu, F., Wang, S., Huang, J., and Hu, L. (2015). Eco-friendly wood-based solid-state flexible supercapacitors from wood transverse section slice and reduced graphene oxide. Electron. Mater. Lett. *11*, 633–642. https://doi.org/10.1007/s13391-015-5023-z.

50. Volperts, A., Dobele, G., Zhurinsh, A., Vervikishko, D., Shkolnikov, E., and Ozolinsh, J. (2017). Wood-based activated carbons for supercapacitor electrodes with sulfuric acid electrolyte. New Carb. Mat. *32*, 319–326. https://doi.org/10.1016/S1872-5805(17)60125-2.

51. Jin, H., Hu, J., Wu, S., Wang, X., Zhang, H., Xu, H., and Lian, K. (2018). Three-dimensional interconnected porous graphitic carbon derived from rice straw for high performance supercapacitors. J. Power Sources *384*, 270–277. https://doi.org/10.1016/j.jpowsour.2018.02.089.

52. Liu, H., Zhao, Q., Wang, K., Lu, Z., Feng, F., and Guo, Y. (2019). Facile synthesis of polypyrrole nanofiber (PPyNF)/NiOx composites by a microwave method and application in supercapacitors. RSC Advances *9*, 6890–6897. https://doi.org/10.1039/c8ra09666j.

53. Lu, J., Lian, F., Guan, L., Zhang, Y., and Ding, F. (2019). Adapting FeS2 micron particles as an electrode material for lithium-ion batteries via simultaneous construction of CNT internal networks and external cages. J. Mater. Chem. A Mater. Energy Sustain. *7*, 991–997. https://doi.org/10.1039/c8ta09955c.

54. Chen, T., Zhang, Z., Cheng, B., Chen, R., Hu, Y., Ma, L., Zhu, G., Liu, J., and Jin, Z. (2017). Self-templated formation of interlaced carbon nanotubes threaded hollow Co_3S_4 nanoboxes for high-rate and heat-resistant lithium-sulfur batteries. J. Am. Chem. Soc. *139*, 12710–12715. https://doi.org/10.1021/jacs.7b06973.

55. Han, Y., Lai, Z., Wang, Z., Yu, M., Tong, Y., and Lu, X. (2018). Designing carbon based supercapacitors with high energy density: A summary of recent progress. Chemistry-a European Journal *24*, 7312–7329. https://doi.org/10.1002/chem.201705555.

56. Lv, S., Fu, F., Guo, L., Chen, Z., and Chang, H. (2017). Microstructure and electrical conductivity of flexible wood slice/nano carbon material composite electrode material. Scie. Silv. Sin. *53*, 150–156. https://doi.org/10.11707/j.1001-7488.20171117.

57. Wan, C., and Li, J. (2016). Wood-derived biochar supported polypyrrole nanoparticles as a free-standing supercapacitor electrode. RSC Advances *6*, 86006–86011. https://doi.org/10.1039/c6ra17044g.

58. Zhao, D., Chen, C., Zhang, Q., Chen, W., Liu, S., Wang, Q., Liu, Y., Li, J., and Yu, H. (2017). High performance, flexible, solid-state supercapacitors based on a renewable and biodegradable mesoporous cellulose membrane. Adv. Energy Mater. *7*, 1700739. https://doi.org/10.1002/aenm.201700739.

59. Jiao, Y., Wan, C., and Li, J. (2017). Scalable synthesis and characterization of free-standing supercapacitor electrode using natural wood as a green substrate to support rod-shaped polyaniline. J. Mater. Sci. Mater. Electron. *28*, 2634–2641. https://doi.org/10.1007/s10854-016-5840-3.

60. Zhang, Y., Shang, Z., Shen, M., Chowdhury, S.P., Ignaszak, A., Sun, S., and Ni, Y. (2019). Cellulose nanofibers/reduced graphene oxide/polypyrrole aerogel electrodes for high-capacitance flexible all-solid-state supercapacitors. ACS Sustain. Chem.& Eng. *7*, 11175–11185. https://doi.org/10.1021/acssuschemeng.9b00321.

61. Xiong, C., Li, M., Nie, S., Dang, W., Zhao, W., Dai, L., and Ni, Y. (2020). Non-carbonized porous lignin-free wood as an effective scaffold to fabricate lignin-free Wood@Polyaniline supercapacitor material for renewable energy storage application. J. Power Sources *471*, 228448. https://doi.org/10.1016/j.jpowsour.2020.228448.

62. Zhu, M., Huang, Y., Deng, Q., Zhou, J., Pei, Z., Xue, Q., Huang, Y., Wang, Z., Li, H., Huang, Q., and Zhi, C. (2016). Highly flexible, freestanding supercapacitor electrode with enhanced performance obtained by hybridizing polypyrrole chains with MXene. Adv. Energy Mater. *6*, 1600969. https://doi.org/10.1002/aenm.201600969.

63. Zang, L., Liu, Q., Qiu, J., Yang, C., Wei, C., Liu, C., and Lao, L. (2017). Design and fabrication of an all-solid-state polymer supercapacitor with highly mechanical flexibility based on polypyrrole hydrogel. ACS Appl. Mater. Interfaces *9*, 33941–33947. https://doi.org/10.1021/acsami.7b10321.

64. Park, H., Kim, J.W., Hong, S.Y., Lee, G., Kim, D.S., Oh, J.H., Jin, S.W., Jeong, Y.R., Oh, S.Y., Yun, J.Y., and Ha, J.S. (2018). Microporous polypyrrole-coated graphene foam for high-performance multifunctional sensors and flexible supercapacitors. Adv. Funct. Mater. *28*, 1707013. https://doi.org/10.1002/adfm.201707013.

65. Zhang, Z., Yu, C., Peng, Z., and Zhong, W. (2021). Mechanically stiff and high-areal-performance integrated all-in-wood supercapacitors with electroactive biomass-based hydrogel. Cellulose *28*, 389–404. https://doi.org/10.1007/s10570-020-03509-8.

66. Peng, Z., Zou, Y., Xu, S., Zhong, W., and Yang, W. (2018). High-performance biomass-based flexible solid-state supercapacitor constructed of pressure-sensitive lignin-based and cellulose hydrogels. ACS Appl. Mater. Interfaces *10*, 22190–22200. https://doi.org/10.1021/acsami.8b05171.

67. Li, F., Wang, X., and Sun, R. (2017). A metal-free and flexible supercapacitor based on redox-active lignosulfonate functionalized graphene hydrogels. J. Mater. Chem. A Mater. Energy Sustain. *5*, 20643–20650. https://doi.org/10.1039/c7ta03789a.

68. Zou, Y., Liu, R., Zhong, W., and Yang, W. (2018). Mechanically robust double-crosslinked network functionalized graphene/polyaniline stiff hydrogels for superior performance supercapacitors. J. Mater. Chem. A Mater. Energy Sustain. *6*, 8568–8578. https://doi.org/10.1039/c8ta00860d.

69. Xia, A., Yu, W., Yi, J., Tan, G., Ren, H., and Liu, C. (2019). Synthesis of porous δ-MnO_2 nanosheets and their supercapacitor performance. J. Electroanal. Chem. (Lausanne) *839*, 25–31. https://doi.org/10.1016/j.jelechem.2019.02.059.

70. Zhang, M., Yang, D., and Li, J. (2021). Ultrasonic and NH4+ assisted Ni foam substrate oxidation to achieve high performance MnO2 supercapacitor. Appl. Surf. Sci. *541*, 148546. https://doi.org/10.1016/j.apsusc.2020.148546.

71. Bai, X.-L., Gao, Y.-L., Gao, Z.-Y., Ma, J.-Y., Tong, X.-L., Sun, H.-B., and Wang, J.A. (2020). Supercapacitor performance of 3D-graphene/MnO2 foam synthesized via the combination of chemical vapor deposition with hydrothermal method. Appl. Phys. Lett. *117*, 183901. https://doi.org/10.1063/5.0018708.

72. Ramesh, S., Kim, H.S., Haldorai, Y., Han, Y.-K., and Kim, J.-H. (2017). Fabrication of nanostructured MnO2/carbon nanotube composite from 3D precursor complex for high-performance supercapacitor. Mater. Lett. *196*, 132–136. https://doi.org/10.1016/j.matlet.2017.03.044.

73. Wang, X., Chen, S., Li, D., Sun, S., Peng, Z., Komarneni, S., and Yang, D. (2018). Direct interfacial growth of MnO2 nanostructure on hierarchically porous carbon for high-performance asymmetric supercapacitors. ACS Sustain. Chem. Eng. *6*, 633–641. https://doi.org/10.1021/acssuschemeng.7b02960.

74. Xie, W.L., Sun, M.Y., Li, Y.Q., Zhang, B., Lang, X.Y., Zhu, Y.F., and Jiang, Q. (2019). Three-dimensional Ni/MnO2 nanocylinder array

with high capacitance for supercapacitors. Results Phys. *12*, 1411–1416. https://doi.org/10.1016/j.rinp.2019.01.041.

75. Chen, C., Zhang, Y., Li, Y., Dai, J., Song, J., Yao, Y., Gong, Y., Kierzewski, I., Xie, J., and Hu, L. (2017). All-wood, low tortuosity, aqueous, biodegradable supercapacitors with ultra-high capacitance. Energy Environ. Sci. *10*, 538–545. https://doi.org/10.1039/c6ee03716j.

76. Gao, S., Sun, Y., Lei, F., Liang, L., Liu, J., Bi, W., Pan, B., and Xie, Y. (2014). Ultrahigh energy density realized by a single-layer β-Co(OH)2 all-solid-state asymmetric supercapacitor. Angew. Chem. Int. Ed. Engl. *53*, 12789–12793. https://doi.org/10.1002/anie.201407836.

77. Xia, X.H., Tu, J.P., Zhang, Y.Q., Mai, Y.J., Wang, X.L., Gu, C.D., and Zhao, X.B. (2011). Three-dimentional porous nano-Ni/Co(OH)(2) nanoflake composite film: A pseudocapacitive material with superior performance. J. Phys. Chem. C *115*, 22662–22668. https://doi.org/10.1021/jp208113j.

78. Wang, Y., Lin, X., Liu, T., Chen, H., Chen, S., Jiang, Z., Liu, J., Huang, J., and Liu, M. (2018). Wood-derived hierarchically porous electrodes for high-performance all-solid-state supercapacitors. Adv. Funct. Mater. *28*, 1806207. https://doi.org/10.1002/adfm.201806207.

79. Zhang, Q., Liu, Z., Zhao, B., Cheng, Y., Zhang, L., Wu, H.-H., Wang, M.-S., Dai, S., Zhang, K., Ding, D., et al. (2019). Design and understanding of dendritic mixed-metal hydroxide nanosheets@N-doped carbon nanotube array electrode for high-performance asymmetric supercapacitors. Energy Storage Mater. *16*, 632–645. https://doi.org/10.1016/j.ensm.2018.06.026.

80. Luo, J., Yuan, W., Huang, S., Zhao, B., Chen, Y., Liu, M., and Tang, Y. (2018). From checkerboard-like sand barriers to 3D Cu@CNF composite current collectors for high-performance batteries. Adv. Sci. (Weinh.) *5*, 1800031. https://doi.org/10.1002/advs.201800031.

81. Li, Z., Li, Y., Wang, L., Cao, L., Liu, X., Chen, Z., Pan, D., and Wu, M. (2017). Assembling nitrogen and oxygen co-doped graphene quantum dots onto hierarchical carbon networks for all-solid-state flexible supercapacitors. Electrochim. Acta *235*, 561–569. https://doi.org/10.1016/j.electacta.2017.03.147.

82. Zhang, W., Yang, Y., Xia, R., Li, Y., Zhao, J., Lin, L., Cao, J., Wang, Q., Liu, Y., and Guo, H. (2020). Graphene-quantum-dots-induced MnO_2 with needle-like nanostructure grown on carbonized wood as advanced electrode for supercapacitors. Carbon *162*, 114–123. https://doi.org/10.1016/j.carbon.2020.02.039.

83. Xin, F., Jia, Y., Sun, J., Dang, L., Liu, Z., and Lei, Z. (2018). Enhancing the capacitive performance of carbonized wood by growing FeOOH nanosheets and poly(3,4-ethylenedioxythiophene) coating. ACS Appl. Mater. Interfaces *10*, 32192–32200. https://doi.org/10.1021/acsami.8b11069.

84. Chen, H., Zhu, X., Chang, Y., Cai, J., and Zhao, R. (2018). 3D flower-like CoS hierarchitectures recycled from spent LiCoO2 batteries and its application in electrochemical capacitor. Mater. Lett. *218*, 40–43. https://doi.org/10.1016/j.matlet.2018.01.144.

85. Ashok Kumar, K., Pandurangan, A., Arumugam, S., and Sathiskumar, M. (2019). Effect of bi-functional hierarchical flower-like CoS nanostructure on its interfacial charge transport kinetics, magnetic and electrochemical behaviors for supercapacitor and DSSC applications. Sci. Rep. *9*, 1228. https://doi.org/10.1038/s41598-018-37463-0.

86. Xiong, C., Li, B., Dang, W., Zhao, W., Duan, C., Dai, L., and Ni, Y. (2020). Co/CoS nanofibers with flower-like structure immobilized in carbonated porous wood as bifunctional material for high-performance supercapacitors and catalysts. Mater. Des. *195*, 108942. https://doi.org/10.1016/j.matdes.2020.108942.

87. Liu, Y., Sun, J., Lin, S., Xu, Z., and Li, L. (2020). *In-situ* growth of interconnected NiS2/MoS2 nanowires supported on Ni foam as binder-free electrode for hybrid supercapacitor. J. Alloys Compd. *820*, 153113. https://doi.org/10.1016/j.jallcom.2019.153113.

88. Sekhar, S.C., Nagaraju, G., and Yu, J.S. (2018). High-performance pouch- type hybrid supercapacitor based on hierarchical NiO-Co3O4-NiO composite nanoarchitectures as an advanced electrode material. Nano Energy *48*, 81–92. https://doi.org/10.1016/j.nanoen.2018.03.037.

89. Sekhar, S.C., Nagaraju, G., and Yu, J.S. (2017). Conductive silver nanowires-fenced carbon cloth fibers-supported layered double hydroxide nanosheets as a flexible and binder-free electrode for high-performance asymmetric supercapacitors. Nano Energy *36*, 58–67. https://doi.org/10.1016/j.nanoen.2017.04.019.

90. Xiong, C., Li, B., Liu, H., Zhao, W., Duan, C., Wu, H., and Ni, Y. (2020). A smart porous wood-supported flower-like NiS/Ni conjunction with vitrimer co-effect as a multifunctional material with reshaping, shape-memory, and self-healing properties for applications in high-performance supercapacitors, catalysts, and sensors. J. Mater. Chem. A Mater. Energy Sustain. *8*, 10898–10908. https://doi.org/10.1039/d0ta03664a.

91. Lu, W., Shen, J., Zhang, P., Zhong, Y., Hu, Y., and Lou, X.W.D. (2019). Construction of CoO/Co-Cu-S hierarchical tubular heterostructures for hybrid supercapacitors. Angew. Chem. Int. Ed. Engl. *58*, 15441–15447. https://doi.org/10.1002/anie.201907516.

92. Liu, S., Gao, D., Li, J., San Hui, K., Yin, Y., Hui, K.N., and Jun, S.C. (2019). Phosphorus dual-site driven CoS2@S, N co-doped porous carbon nanosheets for flexible quasi-solid-state supercapacitors. J. Mater. Chem. A Mater. Energy Sustain. *7*, 26618–26630. https://doi.org/10.1039/c9ta09646a.

93. Parveen, N., Ansari, S.A., Ansari, S.G., Fouad, H., Abd El-Salam, N.M., and Cho, M.H. (2018). Solid-state symmetrical supercapacitor based on hierarchical flower-like nickel sulfide with shape-controlled morphological evolution. Electrochim. Acta *268*, 82–93. https://doi.org/10.1016/j.electacta.2018.01.100.

94. Armand, M., and Tarascon, J.M. (2008). Building better batteries. Nature *451*, 652–657. https://doi.org/10.1038/451652a.

95. Bruce, P.G., Freunberger, S.A., Hardwick, L.J., and Tarascon, J.-M. (2011). Li-O2 and Li-S batteries with high energy storage. Nat. Mater. *11*, 19–29. https://doi.org/10.1038/nmat3191.

96. Pan, H., Hu, Y.-S., and Chen, L. (2013). Room-temperature stationary sodium-ion batteries for large-scale electric energy storage. Energy Environ. Sci. *6*, 2338–2360. https://doi.org/10.1039/c3ee40847g.

97. Zhang, J., Sun, B., Zhao, Y., Kretschmer, K., and Wang, G. (2017). Modified tetrathiafulvalene as an organic conductor for improving performances of Li-O_2 batteries. Angew. Chem. Int. Ed. Engl. *56*, 8505–8509. https://doi.org/10.1002/anie.201703784.

98. Sun, B., Huang, X., Chen, S., Munroe, P., and Wang, G. (2014). Porous graphene nanoarchitectures: an efficient catalyst for low charge-overpotential, long life, and high capacity lithium-oxygen batteries. Nano Lett. *14*, 3145–3152. https://doi.org/10.1021/nl500397y.

99. Fang, H., Gao, S., Zhu, Z., Ren, M., Wu, Q., Li, H., and Li, F. (2021). Recent progress and perspectives of sodium metal anodes for rechargeable batteries. Chem. Res. Chin. Univ. *37*, 189–199. https://doi.org/10.1007/s40242-021-0449-3.

100. Tian, H., Shao, H., Chen, Y., Fang, X., Xiong, P., Sun, B., Notten, P.H.L., and Wang, G. (2019). Ultra-stable sodium metal-iodine batteries enabled by an in-situ solid electrolyte interphase. Nano Energy *57*, 692–702. https://doi.org/10.1016/j.nanoen.2018.12.084.

101. Bommier, C., and Ji, X. (2015). Recent development on anodes for Na-ion batteries. Isr. J. Chem. *55*, 486–507. https://doi.org/10.1002/ijch.201400118.

102. Stevens, D., and Dahn, J. (2000). High capacity anode materials for rechargeable sodium-ion batteries. J. Electrochem. Soc. *147*, 1271. https://doi.org/10.1016/j.dld.2004.05.016.

103. Lotfabad, E.M., Ding, J., Cui, K., Kohandehghan, A., Kalisvaart, W.P., Hazelton, M., and Mitlin, D. (2014). High-density sodium and lithium ion battery anodes from banana peels. ACS Nano *8*, 7115–7129. https://doi.org/10.1021/nn502045y.

104. Li, W., Zeng, L., Yang, Z., Gu, L., Wang, J., Liu, X., Cheng, J., and Yu, Y. (2014). Free-standing and binder-free sodium-ion electrodes with ultralong cycle life and high rate performance based on porous carbon nanofibers. Nanoscale *6*, 693–698. https://doi.org/10.1039/c3nr05022j.

105. Cao, Y., Xiao, L., Sushko, M.L., Wang, W., Schwenzer, B., Xiao, J., Nie, Z., Saraf, L.V., Yang, Z., and Liu, J. (2012). Sodium ion insertion in hollow carbon nanowires for battery applications. Nano Lett. *12*, 3783–3787. https://doi.org/10.1021/nl3016957.

106. Shen, F., Luo, W., Dai, J., Yao, Y., Zhu, M., Hitz, E., Tang, Y., Chen, Y., Sprenkle, V.L., Li, X., and Hu, L. (2016). Ultra-thick, low-tortuosity, and mesoporous wood carbon anode for high-

performance sodium-ion batteries. Adv. Energy Mater. *6*, 1600377. https://doi.org/10.1002/aenm.201600377.

107. Zheng, Y., Lu, Y., Qi, X., Wang, Y., Mu, L., Li, Y., Ma, Q., Li, J., and Hu, Y.-S. (2019). Superior electrochemical performance of sodium-ion full-cell using poplar wood derived hard carbon anode. Energy Storage Mater. *18*, 269–279. https://doi.org/10.1016/j.ensm.2018.09.002.

108. Zhang, X., Yang, Y., and Zhou, Z. (2020). Towards practical lithium-metal anodes. Chem. Soc. Rev. *49*, 3040–3071. https://doi.org/10.1039/c9cs00838a.

109. Wang, R., Cui, W., Chu, F., and Wu, F. (2020). Lithium metal anodes: Present and future. Journal of Energy Chemistry *48*, 145–159. https://doi.org/10.1016/j.jechem.2019.12.024.

110. Hu, Z., Li, J., Zhang, X., and Zhu, Y. (2020). Strategies to improve the performance of Li metal anode for rechargeable batteries. Front Chem. *8*, 409. https://doi.org/10.3389/fchem.2020.00409.

111. Li, C., Lan, Q., Yang, Y., Shao, H., and Zhan, H. (2019). Flexible artificial solid electrolyte interphase formed by 1,3-dioxolane oxidation and polymerization for metallic lithium anodes. ACS Appl. Mater. Interfaces *11*, 2479–2489. https://doi.org/10.1021/acsami.8b16080.

112. Li, N.-W., Shi, Y., Yin, Y.-X., Zeng, X.-X., Li, J.-Y., Li, C.-J., Wan, L.-J., Wen, R., and Guo, Y.-G. (2018). A flexible solid electrolyte interphase layer for long-life lithium metal anodes. Angew. Chem. Int. Ed. Engl. *57*, 1505–1509. https://doi.org/10.1002/anie.201710806.

113. Basile, A., Bhatt, A.I., and O'Mullane, A.P. (2016). Stabilizing lithium metal using ionic liquids for long-lived batteries. Nat. Commun. *7*, s11794. https://doi.org/10.1038/ncomms11794.

114. Yang, C., Gao, Q., Tian, W., Tan, Y., Zhang, T., Yang, K., and Zhu, L. (2014). Superlow load of nanosized MnO on a porous carbon matrix from wood fibre with superior lithium ion storage performance. J. Mater. Chem. A Mater. Energy Sustain. *2*, 19975–19982. https://doi.org/10.1039/c4ta04471a.

115. Zhang, Y., Luo, W., Wang, C., Li, Y., Chen, C., Song, J., Dai, J., Hitz, E.M., Xu, S., Yang, C., et al. (2017). High-capacity, low-tortuosity, and channel-guided lithium metal anode. Proc. Natl. Acad. Sci. USA *114*, 3584–3589. https://doi.org/10.1073/pnas.1618871114.

116. Chen, C., Xu, S., Kuang, Y., Gan, W., Song, J., Chen, G., Pastel, G., Liu, B., Li, Y., Huang, H., and Hu, L. (2019). Nature-inspired tri-pathway design enabling high-performance flexible Li-O_2 batteries. Adv. Energy Mater. *9*, 1802964. https://doi.org/10.1002/aenm.201802964.

117. Manthiram, A., and Li, L. (2015). Hybrid and aqueous lithium-air batteries. Adv. Energy Mater. *5*, 1401302. https://doi.org/10.1002/aenm.201401302.

118. Luo, Z., Li, F., Hu, C., Yin, L., Li, D., Ji, C., Zhuge, X., Zhang, K., and Luo, K. (2021). Highly dispersed silver nanoparticles for performance-enhanced lithium oxygen batteries. J. Mater. Sci. Technol. *73*, 171–177. https://doi.org/10.1016/j.jmst.2020.07.039.

119. Hu, A., Zhou, M., Lei, T., Hu, Y., Du, X., Gong, C., Shu, C., Long, J., Zhu, J., Chen, W., et al. (2020). Optimizing redox reactions in aprotic lithium-sulfur batteries. Adv. Energy Mater. *10*, 2002180. https://doi.org/10.1002/aenm.202002180.

120. Li, L., Han, W., Pi, L., Niu, P., Han, J., Wang, C., Su, B., Li, H., Xiong, J., Bando, Y., and Zhai, T. (2019). Emerging in-plane anisotropic two-dimensional materials. Infomat *1*, 54–73. https://doi.org/10.1002/inf2.12005.

121. Zhang, Z., Bai, W.-L., Wang, K.-X., and Chen, J.-S. (2020). Electrocatalyst design for aprotic Li-CO2 batteries. Energy Environ. Sci. *13*, 4717–4737. https://doi.org/10.1039/d0ee03058a.

122. Xiao, X., Tan, P., Zhu, X., Dai, Y., Cheng, C., and Ni, M. (2020). Investigation on the discharge and charge behaviors of Li-CO2 batteries with carbon nanotube electrodes. ACS Sustain. Chem. Eng. *8*, 9742–9750. https://doi.org/10.1021/acssuschemeng.0c01863.

123. Cai, F., Hu, Z., and Chou, S.-L. (2018). Progress and future perspectives on Li(Na)-CO2 Batteries. Advanced Sustainable Systems *2*, 1800060. https://doi.org/10.1002/adsu.201800060.

124. Ahmadiparidari, A., Warburton, R.E., Majidi, L., Asadi, M., Chamaani, A., Jokisaari, J.R., Rastegar, S., Hemmat, Z., Sayahpour, B., Assary, R.S., et al. (2019). A long-cycle-life Lithium-CO_2 battery with carbon neutrality. Adv. Mater. *31*, e1902518. https://doi.org/10.1002/adma.201902518.

125. Zhao, H., Li, D., Li, H., Tamirat, A.G., Song, X., Zhang, Z., Wang, Y., Guo, Z., Wang, L., and Feng, S. (2019). Ru nanosheet catalyst supported by three-dimensional nickel foam as a binder-free cathode for Li-CO2 batteries. Electrochim. Acta *299*, 592–599. https://doi.org/10.1016/j.electacta.2019.01.027.

126. Liu, B., Sun, Y., Liu, L., Chen, J., Yang, B., Xu, S., and Yan, X. (2019). Recent advances in understanding Li-CO2 electrochemistry. Energy Environ. Sci. *12*, 887–922. https://doi.org/10.1039/c8ee03417f.

127. Hu, A., Shu, C., Xu, C., Liang, R., Li, J., Zheng, R., Li, M., and Long, J. (2019). Design strategies toward catalytic materials and cathode structures for emerging Li-CO2 batteries. J. Mater. Chem. A Mater. Energy Sustain. *7*, 21605–21633. https://doi.org/10.1039/c9ta06506g.

128. Xiao, X., Shang, W., Yu, W., Ma, Y., Tan, P., Chen, B., Kong, W., Xu, H., and Ni, M. (2020). Toward the rational design of cathode and electrolyte materials for aprotic Li-CO2 batteries: A numerical investigation. Int. J. Energy Res. *44*, 496–507. https://doi.org/10.1002/er.4952.

129. Xu, S., Chen, C., Kuang, Y., Song, J., Gan, W., Liu, B., Hitz, E.M., Connell, J.W., Lin, Y., and Hu, L. (2018). Flexible lithium-CO2 battery with ultrahigh capacity and stable cycling. Energy Environ. Sci. *11*, 3231–3237. https://doi.org/10.1039/c8ee01468j.

130. Jiao, M., Liu, T., Chen, C., Yue, M., Pastel, G., Yao, Y., Xie, H., Gan, W., Gong, A., Li, X., and Hu, L. (2020). Holey three-dimensional wood-based electrode for vanadium flow batteries. Energy Storage Mater. *27*, 327–332. https://doi.org/10.1016/j.ensm.2020.02.008.

131. Kim, H., Guccini, V., Lu, H., Salazar-Alvarez, G., Lindbergh, G., and Cornell, A. (2019). Lithium Ion battery separators based on carboxylated cellulose nanofibers from wood. ACS Appl. Energy Mater. *2*, 1241–1250. https://doi.org/10.1021/acsaem.8b01797.

132. Zhang, J., Jiang, G., Xu, P., Kashkooli, A.G., Mousavi, M., Yu, A., and Chen, Z. (2018). An all-aqueous redox flow battery with unprecedented energy density. Energy Environ. Sci. *11*, 2010–2015. https://doi.org/10.1039/c8ee00686e.

133. Yang, Z., Tong, L., Tabor, D.P., Beh, E.S., Goulet, M.-A., De Porcellinis, D., Aspuru-Guzik, A., Gordon, R.G., and Aziz, M.J. (2018). Alkaline benzoquinone aqueous flow battery for large-scale storage of electrical energy. Adv. Energy Mater. *8*, 1702056. https://doi.org/10.1002/aenm.201702056.

134. Sheng, J., Mukhopadhyay, A., Wang, W., and Zhu, H. (2019). Recent advances in the selective membrane for aqueous redox flow batteries. Materials Today Nano *7*, 100044. https://doi.org/10.1016/j.mtnano.2019.100044.

135. Abdalla, A.M., Hossain, S., Nisfindy, O.B., Azad, A.T., Dawood, M., and Azad, A.K. (2018). Hydrogen production, storage, transportation and key challenges with applications: A review. Energy Convers. Manage. *165*, 602–627. https://doi.org/10.1016/j.enconman.2018.03.088.

136. Chen, X., Liu, G., Zheng, W., Feng, W., Cao, W., Hu, W., and Hu, P. (2016). Vertical 2D MoO2/MoSe2 core-shell nanosheet arrays as high-performance electrocatalysts for hydrogen evolution reaction. Adv. Funct. Mater. *26*, 8537–8544. https://doi.org/10.1002/adfm.201603674.

137. Guo, X., Cao, G.-l., Ding, F., Li, X., Zhen, S., Xue, Y.-f., Yan, Y.-m., Liu, T., and Sun, K.-n. (2015). A bulky and flexible electrocatalyst for efficient hydrogen evolution based on the growth of MoS2 nanoparticles on carbon nanofiber foam. J. Mater. Chem. A Mater. Energy Sustain. *3*, 5041–5046. https://doi.org/10.1039/c5ta00087d.

138. Huang, W., Su, S., Liu, Y., Li, J., Wang, M., Hou, Z., Gao, X., Wang, X., Notzel, R., Zhou, G., et al. (2021). Wood-derived electrode supporting CVD-grown ReS(2)for efficient and stable hydrogen production. J. Mater. Sci. *56*, 1551–1560. https://doi.org/10.1007/s10853-020-05248-4.

139. Tian, X., Zhao, P., and Sheng, W. (2019). Hydrogen evolution and oxidation: mechanistic studies and material advances. Adv. Mater. *31*, e1808066. https://doi.org/10.1002/adma.201808066.